UNCLASSIFIED

AD 256 899

Reproduced
by the

ARMED SERVICES TECHNICAL INFORMATION AGENCY
ARLINGTON HALL STATION
ARLINGTON 12, VIRGINIA

UNCLASSIFIED

BEST
AVAILABLE COPY

NOTICE: When government or other drawings, specifications or other data are used for any purpose other than in connection with a definitely related government procurement operation, the U. S. Government thereby incurs no responsibility, nor any obligation whatsoever; and the fact that the Government may have formulated, furnished, or in any way supplied the said drawings, specifications, or other data is not to be regarded by implication or otherwise as in any manner licensing the holder or any other person or corporation, or conveying any rights or permission to manufacture, use or sell any patented invention that may in any way be related thereto.

AD No. 256 899
ASTIA FILE COPY

4

METEOROLOGICAL SATELLITE SYSTEM ANALYSES

GERALD COOPER

ALLIED RESEARCH ASSOCIATES, INC.
43 LEON STREET · BOSTON 15, MASSACHUSETTS

24 DECEMBER 1959

FIRST SEMI-ANNUAL TECHNICAL SUMMARY REPORT

UNDER

CONTRACT NO. AF 19(604)-5582

ARPA ORDER NO. 26-59

ARPA PROJECT CODE NO. 2600

GEOPHYSICS RESEARCH DIRECTORATE
AIR FORCE CAMBRIDGE RESEARCH CENTER
AIR RESEARCH AND DEVELOPMENT COMMAND
UNITED STATES AIR FORCE BEDFORD, MASSACHUSETTS

METEOROLOGICAL SATELLITE SYSTEM ANALYSES

GERALD COOPER

ALLIED RESEARCH ASSOCIATES, INC.
43 LEON STREET · BOSTON 15, MASSACHUSETTS

24 DECEMBER 1959

FIRST SEMI-ANNUAL TECHNICAL SUMMARY REPORT

UNDER

CONTRACT NO. AF 19(604)-5582

ARPA ORDER NO. 26-59

ARPA PROJECT CODE NO. 2600

GEOPHYSICS RESEARCH DIRECTORATE
AIR FORCE CAMBRIDGE RESEARCH CENTER
AIR RESEARCH AND DEVELOPMENT COMMAND
UNITED STATES AIR FORCE BEDFORD, MASSACHUSETTS

FOREWORD

The research resulting in this report was performed by Allied Research Associates, Inc., Boston, Massachusetts, and was sponsored by the Geophysics Research Directorate, Air Force Cambridge Research Center, Air Research and Development Command, under Contract No. AF 19(604)-5582, through support provided under Advanced Research Projects Agency Order No. 26-59.

This report contains contributions from a number of authors. A. L. Goldshlak contributed Section 2.1, A Survey of Applications of Meteorological Satellites; R. J. Boucher contributed Section 3.1, A Photogrammetric Method of Obtaining the Camera Axis and Its Application in Determining the Time of Photographs Taken From a Space Vehicle; Dr. R. Wexler contributed Section 4.1, Detection of Ozone Amounts from Satellite Measurements; and Dr. A. H. Glaser and Dr. S. N. Milford contributed Section 4.2, A Preliminary Investigation of the Infrared View of the Earth's Atmosphere from a Satellite. The editing and introductory material were provided by Dr. A. H. Glaser and G. Cooper.

ABSTRACT

A literature survey of possible meteorological satellite applications has been made to define some of the information requirements of the meteorological consumer. An attempt was made to appreciate the problems involved in transmitting such information to the meteorological consumer by examining some photographs of the earth taken from an Atlas nose cone. Difficulties encountered in processing these photographs led to the development of a technique for establishing the camera axis azimuth and time of photograph from landmarks when other data cannot supply this information.

Some study was devoted to determining the type of meteorological information that can be developed by using sensors which detect ultraviolet and infrared radiation rather than the visible radiation detected in photographs. In this connection, a method for determining atmospheric ozone amounts by measuring the scattered radiation at two different wave lengths in the ultraviolet has been investigated to determine the theoretical ratios of radiation intensities to be expected. In addition, the view of the earth's atmosphere in an infrared water absorption band has been examined and found to correspond to a picture of the temperature of a constant dew point surface. Some of these constant dewpoint surfaces have been analyzed in connection with the corresponding conventional surface and upper air weather maps and indicate the existence of interesting meteorological relationships which should be studied further.

TABLE OF CONTENTS

LIST OF ILLUSTRATIONS

SECTION I

INTRODUCTION

A meteorological satellite system may be viewed as a connecting link between the real atmosphere and an operational or research user of meteorological information. It is primarily distinguished from other weather observing systems by the use of the satellite as a vehicle for carrying the meteorological sensors, and by having the sensing elements remote from the atmosphere. Other distinctions between a meteorological satellite system and conventional weather observing systems are natural consequences of the vehicle properties.

Recognizing that a meteorological satellite system is a weather observing system, it is clear that its only purpose is to abstract information from the atmosphere and transfer it to the consumer of the information. The information presented to the consumer is only useful insofar as it serves a purpose. Ideally, the meteorologist should always have available the appropriate information to permit a definitive answer to each decision that may be required. Any information provided beyond this requirement is superfluous.

The function of the satellite meteorological system is thus to abstract from the atmosphere those events which are of importance to the activities of the consumer and to transmit to the consumer information on those events in unambiguous fashion. The most efficient and effective system will be the one that provides this service and no more. Appropriate system design will thus depend on detailed knowledge of the needs of the meteorological consumer and knowledge of the observational material available from the atmosphere to satisfy these needs. Actual design of the system then becomes a matter of arranging the transfer of this information in the most expeditious fashion.

Accordingly, this analysis of meteorological satellite systems is devoted to an examination of the various aspects of the information transfer process. Starting at the consumer and working back towards the information source in the atmosphere, the information transfer process may be divided into the following broad categories of study purposes:

A – Applications of Meteorological Satellites

B – Data Processing and Interpretation

C – Data Storage and Transmission

D – Orbital Sampling Characteristics

E – Sensors and Sensor Techniques

To date, the study program has been concerned with items A, B, and E, following an approach which starts at both ends of the information transfer process and works towards the middle. In order to understand better the requirements of the meteorological consumer, a continuing survey is being made of the possible applications of satellite meteorology.

To appreciate better the problems of data processing and interpretation, photographs of weather features on the earth taken at satellite altitudes during a ballistic flight of an Atlas nose cone were examined. From this examination, it became apparent that minor instrumentation failures might cause difficulties in establishing the orientation of the satellite and the time at which the photographs were taken. A technique is described which may be useful in obtaining such information in certain cases. Further pertinent work in processing satellite photographic data has been done by Allied Research Associates, Inc. under Contract No. AF 19(604)-5581 under the same sponsorship. It is described in a report to be released simultaneously with the present work.

Turning to the area of sensors and sensor techniques, it was recognized that a great amount of work has already been done on optical sensors. Accordingly, some preliminary study was devoted to determining the utility of ultraviolet sensors in an ozone absorption band and infrared sensors in a water absorption band.

The material presented here leads toward an integrated survey which will serve as basic material for the design of meteorological satellite systems.

SECTION II

APPLICATIONS OF METEOROLOGICAL SATELLITES

To establish the requirements of the consumer of meteorological satellite data, it is necessary to investigate the possible applications of such data. Since there is an abundant literature in this field, a survey provides a picture of at least some of the consumer information requirements. This literature also provides some suggestions relating to the design of the satellite meteorology system.

2.1 A Survey of Applications of Meteorological Satellites

2.1.1 Introduction

The following section is concerned with some phases of the utilization of a meteorological satellite. Selected material from a literature search has been integrated with the applicable findings and experience obtained from closely associates fields of study at Allied Research. An attempt has been made to avoid extremely generalized and all-inclusive statements about the utilization of a satellite for meteorological investigations.

The meteorological parameters mentioned in Section 2.1.4 contain references to literature which makes some specific suggestions as to methodology and/or instrumentation.

Supplementary and/or complementary information concerning applications for meteorological satellites will be made available in the future. It is anticipated that the TIROS I experiment will provide additional information concerning various aspects of satellite meteorology.

2.1.2 Planetary Parameters

2.1.2.1 The Solar Constant

"The ultimate source of thermal energy for the earth's atmosphere is the incident solar radiation, and we must know its precise form outside the limits of the atmosphere." (Ref. 1). The presently accepted value of the solar constant is approximately 2 ly. min^{-1}. The measurement error is of the order of two percent and is largely attributable to uncertainties in the assumptions used to correct the measurements for atmospheric effects.

An earth satellite, orbiting above the atmosphere, equipped with a bolometer pointing towards the sun could measure the solar constant directly. Daily measurements over a long period of time could provide the research with answers to the following questions: Is the solar constant a true constant? If not, how much does it vary? Observers at the Smithsonian Institute claim that the value of the solar constant actually varies by 1 or 2 percent. This claimed value is of the same order as the present measurement error, and, therefore, cannot be verified through current measurement techniques.

2.1.2.2 The Planetary Albedo

The planetary albedo of the earth "... plays a critical role in the radiation budget of our planet and thus in specifying the manner in which the general circulation of the atmosphere must operate, to balance this budget." (Ref. 2)

Various indirect methods have been used (Ref. 3) in an attempt to determine the planetary albedo. The best determination of the planetary albedo would be accomplished by measuring it directly through extra-terrestrial means. Appropriate photocell sensors mounted on a satellite can provide a direct total albedo value. Godson (Ref. 2) suggests the utilization of a television sensor to determine the visual albedo of the earth. He also suggests an orbit of 4000 miles (period of about 4 hours) with a high resolution system.

2.1.2.3 General Circulation of the Earth

The general circulation of the earth is fundamentally driven by the radiation balance between the earth and outer space. It is suggested by Godson (Ref. 2) that this balance be measured continuously as a function of space and time.

Differentiation between radiation in the various frequencies is necessary for proper interpretation of the radiation balance. A pair of parallel-plate radiometers with surface absorptions which vary with wave length is the satellite instrumentation suggested by Godson.

The energy balance of the earth and atmosphere can be formulated separately if synoptic cloud images are available and the individual energy components of the radiation budget are known.

2.1.2.4 Global Cloud Climatology – Cloud Albedo

The cloud albedo provides the greatest contribution to the planetary albedo. Different types of clouds and cloud combinations contribute in varying amounts to the total cloud albedo, depending on the optical properties of the clouds, cloud thickness and the zenith angle of the sun.

As a result of the importance of cloud albedo, it is strongly urged that a global cloud climatology be assembled (Refs. 4 and 5). To facilitate associated avenues of future research, the cloud climatology should be divided into continental and oceanic areas. Further subdivision into diurnal and seasonal variations are also desirable.

A reconnaissance satellite equipped with relatively simple instrumentation such as a television camera would be adequate for initial studies. Inspection of the photographs taken from the Atlas 11C (24 August 1959) nose cone reveal the feasibility of determining cloud cover over large areas from high-altitude pictures. Figure 1 is a photograph of the earth taken at an altitude of about 450 miles; Figures 2 and 3 were taken from an altitude of about 750 miles over a different sector of the earth. The cloud cover is readily visible on these photographs.

Reliable determination of cloud types would require a high-resolution (at least 1000 lines per frame) television camera. The desired cloud scale and cloud detail would dictate the resolution required as a function of satellite altitude. Minimum orbital heights would be appropriate for observations of cloud types. Cloud cover information may also be obtained from higher orbits.

Fig. 1 CLOUD COVER AS VIEWED FROM AN ATLAS MISSILE AT A HEIGHT OF APPROXIMATELY 450 STATUTE MILES

Fig 2 CLOUD COVER AS VIEWED FROM AN ATLAS MISSILE AT A HEIGHT OF APPROXIMATELY 750 STATUTE MILES

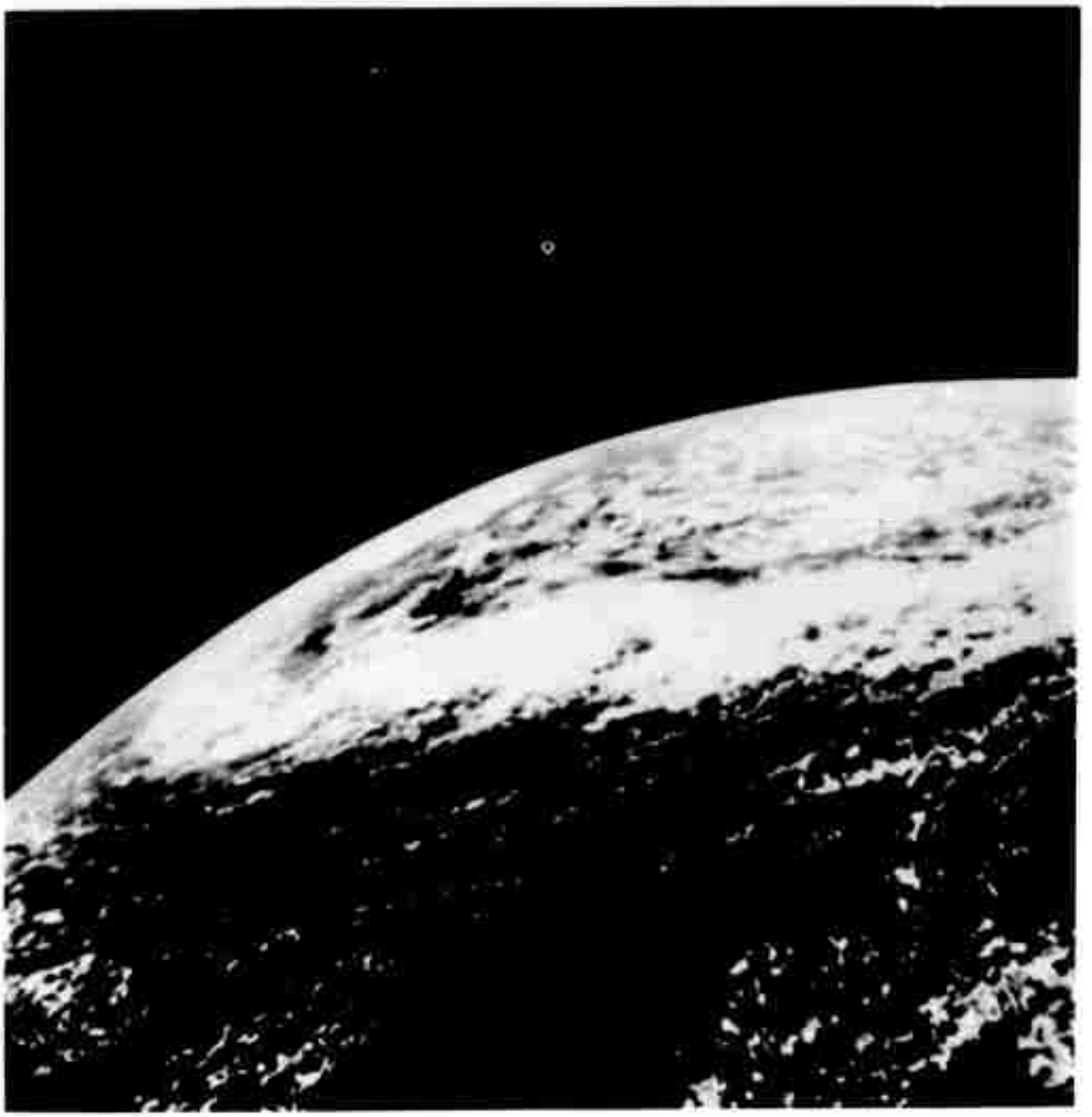

Fig. 3 CLOUD COVER AS VIEWED FROM AN ATLAS MISSILE AT A HEIGHT OF APPROXIMATELY 750 STATUTE MILES

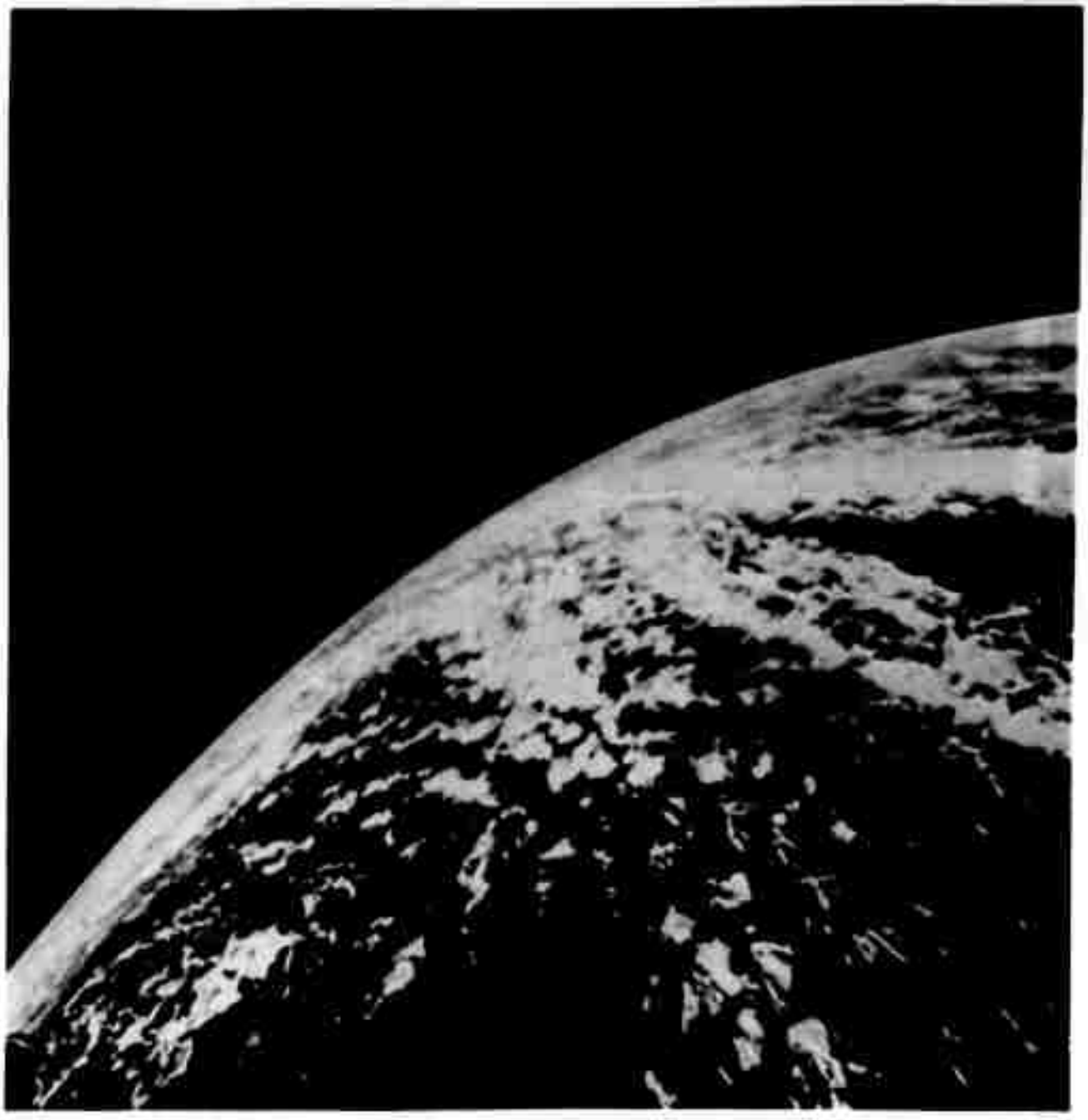

A report by Glaser (Ref. 5) deals with the recognition of cloud forms from a satellite. Of particular interest in that report is the section on the significance of large scale reflectivity patterns. In addition, Glaser has tabulated typical reflectivity values for various cloud cover combinations.

One of the great advantages of utilizing a system of satellites for cloud reconnaissance (as well as for other meteorological parameters) will be the ability to obtain nearly simultaneous measurements over large areas of the earth (Ref. 6). Since the life period of clouds is relatively short and cloud transformations can occur rapidly, the necessity of near instantaneous measurements is desirable. Furthermore, it is extremely difficult, if not impossible for a surface stationed observer to obtain a valid image of an entire cloud system, with the exception of very small-scale or local phenomena.

The photographs shown in Figures 1, 2, and 3 present an entirely novel and most useful image to the meteorologist.

2.1.3 Nephanalysis

Clouds are visible evidence of physical and dynamical processes occurring in the atmosphere. A complete understanding of these processes would probably enable the meteorologist to improve his forecasting techniques to a significant degree.

Unfortunately, the subject of nephanalysis (cloud analysis) has been neglected, resulting in limited use of a potentially fertile research and synoptic tool. Recently, the interest in nephanalysis has revived somewhat, as noted from the growing number of articles appearing in the technical literature.

The photographs obtained from the Atlas 11C missile, as exemplified by Figures 1, 2, and 3, reveal that the cloud patterns are certainly not random. The orderly orientation of cloud patterns in bands and streaks (on many scales) indicate that large-scale cloud formation is controlled by some physical or dynamical processes.

A great quantity of useful data can be extracted from high altitude cloud images (Refs. 4, 5, and 7 through 10) through the utilization of relatively simple instrumentation – i.e., television or photocells.

Admittedly, the initial data reduction will most probably be of the semi-quantitative form. Improved data "quality" may be anticipated with advanced technology. The utilization of cloud data obtained from a satellite will be valued by both the synoptician and the researcher.

A report by Goldshlak, Boucher, and Glaser (Ref. 4) was prepared to organize the miscellaneous aspects of cloud-weather relationships. The form of the report is such that it may be used as a manual for extracting meteorological information from a cloud field. In addition, the report contains a case study, comparing the nephanalysis with conventional synoptic analysis.

Another report by Glaser (Ref. 5) illustrates some of the more quantitative aspects of cloud analysis techniques from high altitude reconnaissance.

No attempt will be made here to repeat all the material available in References 4, 5, and 7. In its place, a tabular listing of the information capable of being extracted from cloud images is presented.

A. Identification of Synoptic Systems
   1. Extra tropical cyclones
   2. Anticyclones
   3. Hurricanes
   4. Fronts
   5. Easterly waves
   6. The westerly trough
   7. Intertropical convergence zone
   8. Squall Lines
   9. Shear line
   10. Thunderstorms

B. Climatologies – Annual, Seasonal, Diurnal
   1. Global cloud atlas
   2. Cloud types
   3. Cloud cover
   4. Source regions of storms
   5. Storm tracks
   6. Snow cover
   7. Atmsopheric pollutants

C. Dynamics
   1. Waves
   2. Convergent areas
   3. Divergent areas
   4. Wind fields – wind shear – jet stream

D. Thermodynamics
   1. Convective areas
   2. Turbulence
   3. Stability
   4. Humidity
   5. Advection

E. Research Requirements
   1. Cloud formation and dissipation
   2. Cloud dynamics
   3. Improved cloud-weather inferences

2.1.4 Some Specific Meteorological Parameters

2.1.4.1 Cloud Velocities

Aiken and Widger (Ref. 11) have reported on the possibility of measuring cloud velocities from cloud images obtained from satellites. The authors have shown that the measurement accuracy required to determine cloud speeds to within $\pm$ 10 miles per hour cannot be obtained in practice. The meteorological value of cloud velocities in error by more than 10 miles per hour is minimal.

Other suggested methods for determining cloud velocities are by the use of parallax or multiple sightings over small time intervals. These require phenomenal accuracy of satellite orientation.

2.1.4.2 Ozone

An interpretation of the vertical distribution of ozone can be made from observations of scattered UV radiation at various wave lengths, since the ozone absorption coefficient (Hartley Band) varies more rapidly with wave length than does the coefficient of molecular scattering.

Singer and Wentworth (Ref. 12) discuss a method for determining the vertical ozone distribution from a satellite, by utilizing the optical absorption properties of ozone near 2900 A^{o}. A method of measuring total ozone mass by a comparison of scattered UV radiation at two wave lengths (3110 A^{o} and 3290 A^{o}) is discussed in Section 4.1 of this report.

Below 30 km, ozone has a relatively long lifetime; therefore, ozone concentrations may be used as an indication of air mass motion.

2.1.4.3 Stability

Cloud street spacing may be used as an indication of the depth of the overturning layer (Ref. 13). In temperate latitudes the presence of streets indicates a lapse rate which is near dry adiabatic from the surface to the cloud level.

2.1.4.4 Temperature

Kaplan (Ref. 14) has outlined a method of determining a three-dimensional distribution of atmospheric temperature by obtaining spectral measurements of radiation in the 15μ carbon dioxide band. The carbon dioxide band is preferred to the water vapor bands because the carbon dioxide in the atmosphere is uniformly distributed, whereas the distribution of water vapor is variable.

The radiation in the far wings of the carbon dioxide spectrum emanates largely from cloud tops or from the ground. Observations of this portion of the spectrum might be obtained with a sensor mounted on a balloon or aircraft at 100 mb or above. However, measurement at the dense center of the band would be pointless at these altitudes since considerable atmosphere still exists at greater heights. A satellite orbits at sufficient altitude so that it can receive the emission from the "effective" top of the atmosphere. Then, the center of the 15μ band could be clearly interpreted as emission from the highest emitting layers of the atmosphere.

After establishing the emission from the top and bottom (ground) of the atmosphere, additional layers within the atmosphere may be determined, since "... different fractions of the black-body radiation are received from the various intervening air layers." (Ref. 14).

The suggested sensing instrument is a multiple-slit or multiple-detector grating spectrometer capable of resolving 10 cm^{-1} at 15μ. Rather complicated calculations are required to reduce these observations to actual temperature distributions.

2.1.4.5 Moisture Distribution

Moisture measurements (Ref. 14) could be made simultaneously and through the same optics as the temperature measurements (see Section 2.1.4.4). The water vapor emission may be interpreted in terms of the moisture distribution once the temperature distribution is known.

Surface and cloud top measurements may be obtained at 11μ; stratospheric humidity from the 24μ peak (with additional detail if measurements can reach 40μ). Humidity at the lower heights can be measured at smaller wave lengths.

Some quantitative aspects of humidity measurements are discussed in Section 4.2 of this report.

2.1.4.6 Visibility

Balloon techniques for determining visual range have been extended for possible utilization on a satellite vehicle. Stakutis and Brennan (Ref. 15) discuss some methods for visual range measurements and required satellite instrumentation. The Weston photronic barrier-layer cell is proposed as the essential portion of the instrumentation. Provisions for increased sensitivity of the sensor elements can be made for adaptation to the higher altitude conditions necessitated by satellite carriers.

Visibility is an air mass characteristic and may, therefore, be used for air mass identification purposes. Visibility may also be utilized as an index of air pollution. A knowledge of visibility conditions have further application in military decisions and transportation.

2.1.4.7 Winds

The report by Goldshlak, Boucher, and Glaser (Ref. 4) presents a case study in which both low- and high-level winds were inferred as a part of the synoptic analysis determined from a mosaic of cloud images. Although

no isolated cloud can, at present, provide conclusive wind information, the meteorologist can make good wind direction inferences from a knowledge of the cloud field associated with synoptic systems.

As an example of wind inferences from cloud patterns, the presence of cumulus cloud streets are indicative of the wind direction (parallel to the streets) at the cloud street levels. However, the wind direction may be ambiguous by 180 degrees. The correct wind direction can usually be established from other significant features.

Widger and Touart (Ref. 16) suggest that some estimates of low-level wind speed and direction may be deduced from visible atmospheric pollutants. Over large water bodies the state of the sea surface may also provide surface wind information.

Although some general methods appear to be available for determining wind directions, the problem of determining wind speeds with sufficient accuracy for meteorological application still exists.

2.1.4.8 Jet Stream

Certain cloud patterns – i.e., banded cirrus or cirrus sheets with sharp edges – may be used as aids in locating the jet stream. "Wide belts of cirrus with a clear space or zone of cirrocumulus between indicates a jet to the north of the northernmost cirrus belt and another just south of the break in the cloud. Pronounced bands of cirrus oriented from the southwest indicate jets which are rapidly moving eastward; 'streaky' cirrus suggests double jets which are not migrating appreciably sidewise." (Ref. 13).

The above statements, extracted from a report by Conover (Ref. 13), may apply only to the section of southern New England, where the observational sites for the investigation were located. Further investigations of a similar nature (throughout the atmosphere) could be most efficiently accomplished by satellite reconnaissance.

2.1.5 Useful Meteorological Orbits

Singer (Ref. 6) considers a polar orbit as one of the most useful for a meteorological satellite. Such an orbit would permit the scanning of the entire earth's surface, thus obtaining global data.

H. Wexler (Ref. 17) suggests that an orbit 4000 miles above the earth's surface would be satisfactory for a television satellite. Full advantage of a high-resolution television camera may then be obtained. It should be pointed out that orbits closer to the earth will probably be necessary, depending on the required observational detail.

Other useful satellite orbits and area of coverage problems are discussed by Dryden (Ref. 18). He states that the apparent longitudinal displacements (on the earth) of an orbit fixed in space may be used advantageously for tracking mid-latitude systems. The variable orbital "... displacements for intervals of time shorter than a period do not seem to be important on a synoptic scale." Of greater importance is the "... varying range of visual observations and the changes in resolution resulting from the varying elevation ..."

SECTION III

DATA PROCESSING AND INTERPRETATION

Presently planned meteorological satellite systems, whose purpose is to obtain cloud photographs, are designed to provide considerable auxiliary information to be used in locating the photographed region. Various techniques for obtaining the map coordinates of the pertinent weather features observed on the photographs have been worked out by Allied Research Associates, Inc. under Contract No. AF 19(604)-5581 and are being reported in the First Semi-Annual Technical Report of that contract. In order to appreciate better the problems of data processing and interpretation, photographs of weather features taken during a ballistic flight of an Atlas missile were examined. In the course of this examination, it was found that lack of sufficient documentation made it impossible to apply directly the techniques for obtaining the map coordinates of weather features. A procedure was devised to develop the necessary data to permit application of the mapping techniques. This procedure is presented here.

3.1 A Photogrammetric Method of Obtaining the Camera Axis and Its Application In Determining the Time of Photographs Taken from a Space Vehicle

3.1.1 Introduction

The technique which will be described below was devised specifically to provide data necessary for the interpretation of pictures taken from the Atlas Missile 11C. However, this technique, or a slightly modified version thereof, may be applied to pictures received from any missile or satellite vehicle for the purpose of providing or verifying data on the azimuths of the principal lines, or camera axes and the times of the pictures.

3.1.2 Description of the Techniques

It is assumed that the missile or satellite will be tracked with sufficient accuracy to establish the position of its subpoint and its height at any given time. The satellite vehicles will also telemeter data, independent of the picture information, which should suffice to determine the angle of the camera and/or spin axis with respect to the subpoint at any given time. It is possible, however, that the orientation of the camera axis and the timing of the pictures, either television or direct photographs, may be in doubt at times due to a number of possible factors affecting the rate of picture taking and the start of picture taking sequences, difficulties in transmission of pictures and other data, or partial or temporary failure of one or several components in either the satellite or read-out stations. This may necessitate determining the relation between the time and space coordinates of the vehicle and its orientation from the pictures themselves.

The first step in the technique is to find pictures with recognizable landmarks such as islands, coastlines or land features which can be identified on a map and which can yield latitudes and longitudes of at least two points along the principal line (the projection of the principal axis on the film plane) of the photograph.

In order to facilitate establishing accurately the principal point and principal line of the photographs, permanent fiducial marks in the optical system are highly desirable. Should these be absent, it may still be possible to establish, with reasonable accuracy, the principal point of the picture. This requires that the square or rectangular boundaries of each picture be determined. Assuming the camera lens to be centered, the principal point is then the intersection of diagonals from opposite corners. This point may be above or below the horizon, depending on the height and nadir angle.

The principal line is drawn, which is defined as a line passing through the principal point and perpendicular to a tangent to the horizon at a point where the principal line intersects the horizon. The second point needed to draw this line can be found by locating two points on the horizon equidistant from the principal point. The desired point defining the principal line will then be the intersection of two more arcs from

each of the horizon points. (See Figure 4). This procedure can be repeated for as many pictures as needed which have recognizable land features falling under the principal line. In the case of the Atlas 11C, suitable pictures were selected from each of the five scans of the camera which were recorded on film, and principal points and principal lines drawn on each.

The next step is to establish the geographical location – i.e., latitude and longitude – of the two or more recognizable landmarks intersected by the principal line, using a set of high quality maps such as may be found in the Times Atlas of the World.

On a Mercator or Transverse Mercator map on which has been plotted successive positions and times of the vehicle subpoint, the landmarks positions are plotted and a line connecting them is extended until it intersects the locus of the vehicle subpoints. The intersection point then furnishes an estimate of the time of this picture and also the subpoint of the vehicle at the time of the picture. There is an obvious source of error in this approximate technique because of the map projection used. A gnomonic projection would result in correct bearings – but this projection is virtually useless for other purposes. However, there is a simple method of correcting for the fact that a bearing line (great circle) on a Mercator map should be a curved and not a straight line. This method, shown in detail in Reference 19, consists of adding or subtracting the "convergency" to the azimuth or bearing. The convergency, C, is computed as follows:

$$C = \Delta 0 \sin \frac{\phi_1 + \phi_2}{2} \qquad (1)$$

where

$\Delta 0$ = difference in longitude between end points of the bearing or azimuth line,

ϕ_1 and ϕ_2 are the latitudes of the end points.

The sign of C will be positive if the vehicle is east of the landmarks used or negative if west. Obviously, C will be zero or near zero when the line crosses the equator and zero when the bearing is along a meridian.

FIG.4 SKETCH SHOWING METHOD OF LOCATING PRINCIPAL LINE ON SPACE VEHICLE PHOTOGRAPH

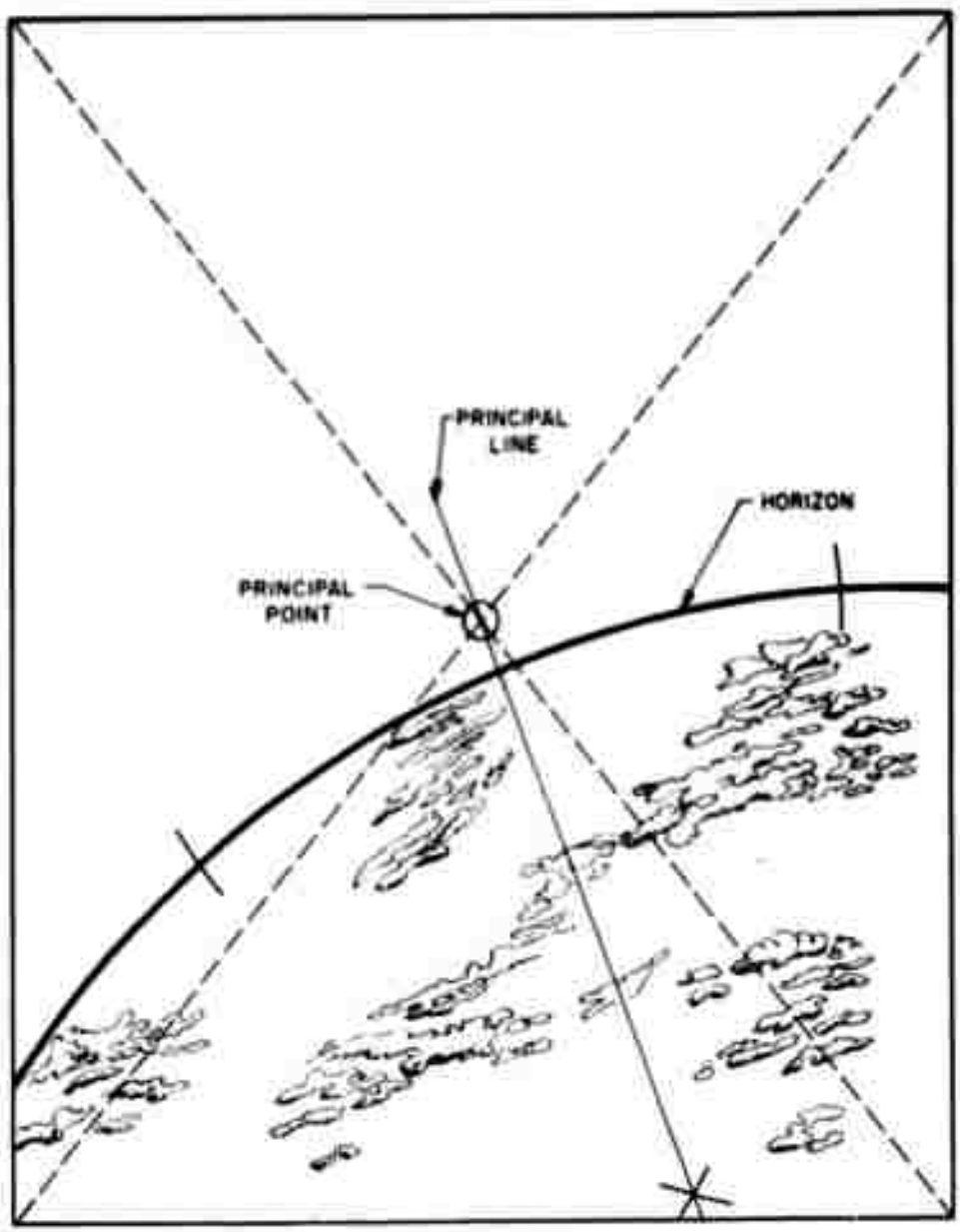

In the case of the Atlas 11C missile pictures, the maximum bearing error was 4° for an E - W bearing at about 27° N. Most errors were of the order of 1° to 2° which is considered within the magnitude range of other errors.

Using the method described above, it then becomes possible to plot frame number versus time for the pictures for which lines can be plotted, as illustrated in Figure 5. If enough reference points are available, a curve can be drawn allowing the determination of time for any frame number.

In a similar manner, the azimuths of the bearings can be plotted against frame number and another curve drawn giving azimuth versus frame number, as shown in Figure 6, which is necessary in establishing the location of clouds observed in the pictures.

3.1.3 Conclusion

The method described above, while devised specifically for use with the Atlas 11C pictures, may be adapted for use with pictures obtained from other vehicles, including satellites. The successful application will hinge on obtaining sufficient pictures with recognizable landmarks. The pictures must have the horizon visible, otherwise the principal line cannot be established.

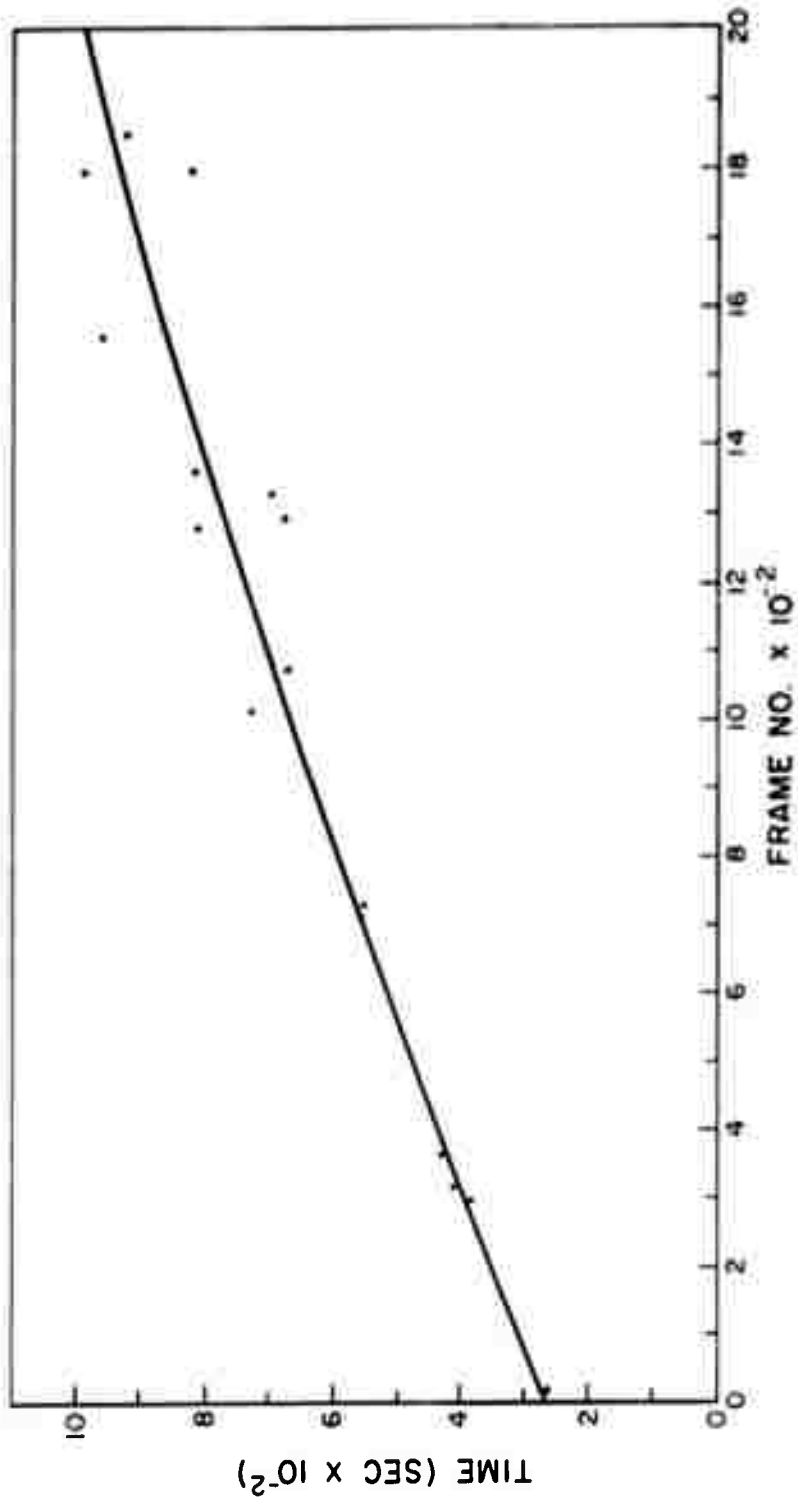

FIG.5 FRAME NUMBER VS TIME FOR ATLAS IIC PHOTOGRAPHS

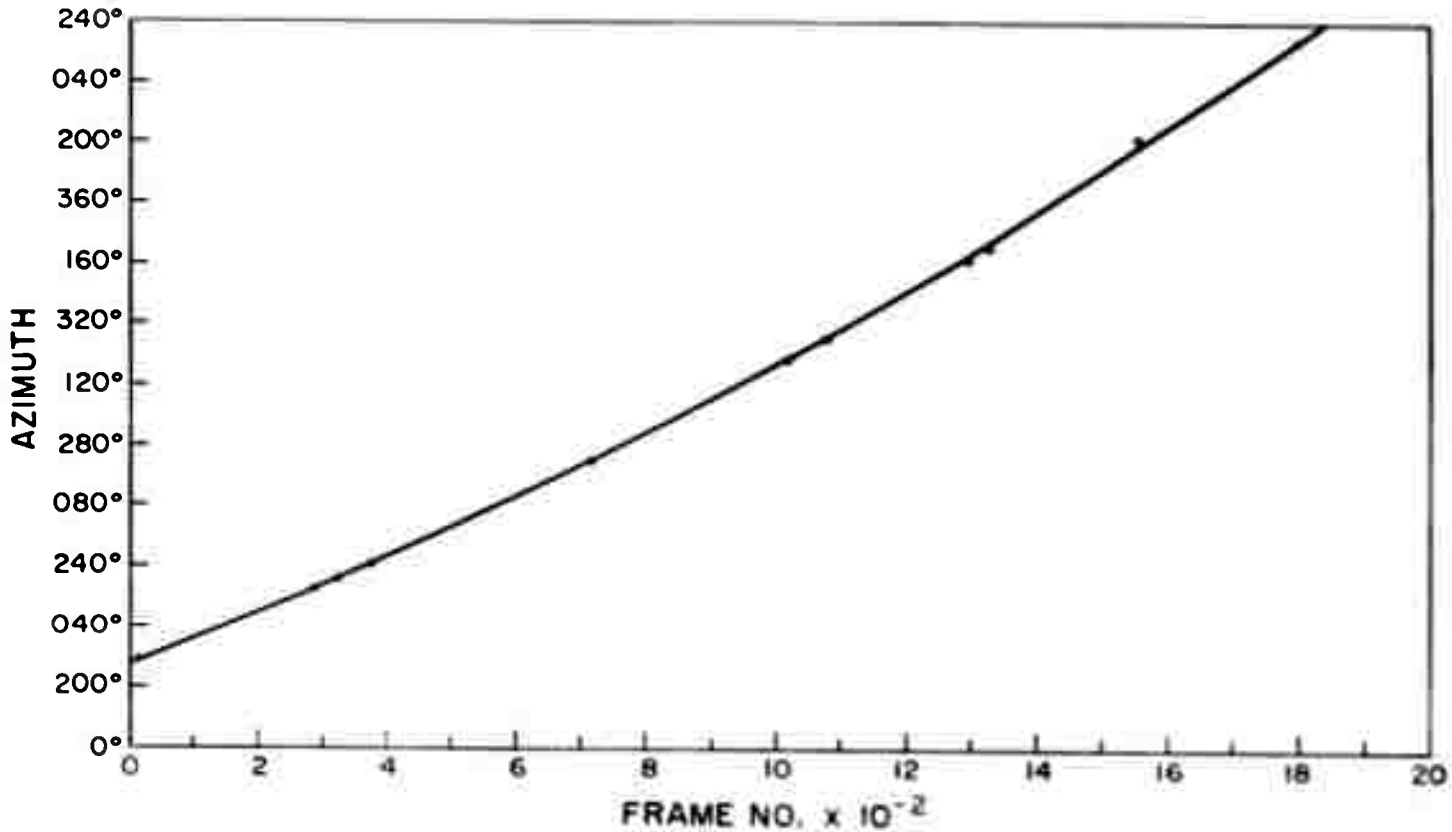

FIG.6 FRAME NUMBER VS AZIMUTH FOR ATLAS IIC PHOTOGRAPHS

SECTION IV

SENSORS AND SENSOR TECHNIQUES

Most of the work done in the field of satellite meteorology has dealt with the use of optical sensors. Since the optical wave lengths form only a very small portion of the electromagnetic energy spectrum, presumably additional information can be obtained from observations at other portions of the spectrum. It appears reasonable to expect that observations in the spectral region where ozone absorption is pronounced would yield information on the ozone distribution in the atmosphere, and observations in a water absorption region would yield information on the water distribution. Accordingly, a somewhat detailed examination was made of the nature of data that would be obtained by observations in the appropriate regions. Section 4. 1 deals with an ultraviolet sensor in the ozone absorption region and Section 4. 2 deals with an infrared sensor in the water absorption region.

4. 1 Detection of Ozone Amounts from Satellite Measurements

4. 1. 1 Introduction

One of the methods used to measure the amount of ozone in the atmosphere is the determination of the intensity of direct solar radiation at two different wave lengths in the ultraviolet, frequently 0. 311μ and 0. 329μ. The former wave length is strongly absorbed and the latter very weakly absorbed by ozone. Measurements at the surface are generally made at different zenith angles, which allows a rough determination of the heights of the ozone layer.

Another method involves measurements of the intensities of the scattered radiation at these wave lengths. Such measurements, generally made with the sun at large zenith angles, result in the well known "umkehr" effect when the ratio of the intensities of the strongly absorbed to that of the weakly absorbed wave lengths reaches a maximum at about sunrise or sunset.

The determination of ozone amounts from a satellite by measuring the scattered radiation from an atmospheric column at two different wave lengths was suggested by Singer (Ref. 6). In this note, this method is discussed in an effort to determine the theoretical ratios of radiation intensities to be expected at the two wave lengths.

4.1.2 Theory

Let the sensor on the satellite be directed at an angle ϕ from the zenith. The solar radiation at angle 0 from the zenith and of intensity I_o at the top of the atmosphere will undergo scattering and absorption in the atmosphere. The scattered radiation towards the satellite will also undergo this attenuation.

Singer (Ref. 6) has shown that the amount of radiation incident at the satellite is theoretically independent of range, although the volume of atmosphere being sampled is directly proportional to the square of the range. The intensity of the solar radiation at depth h from the top of the atmosphere is given by

$$I_{o\lambda}\, e^{-\int_0^h (k_a + k_s) \sec 0 \, dh} \tag{2}$$

where k_a and k_s are the absorption and scattering coefficients respectively. The intensity I_λ of scattered light reaching the outside of the atmosphere is given by the equation

$$\frac{I_\lambda}{I_{o\lambda}} = \int_0^h S\, e^{-\int_0^h (k_a + k_s) X \, dh} \sec \phi \, dh \tag{3}$$

where S is the ratio of scattered to incident radiation from a unit volume of air in the direction ϕ, and $X = \sec 0 + \sec \phi$ is the slant path length correction factor.

Assume now that the absorption due to ozone takes place outside the atmosphere and so is independent of h. This is not a serious restriction since the ozonosphere is located above about 95% of the atmosphere. Then

$$\frac{I_\lambda}{I_{o\lambda}} = e^{-k_a m X} \int_0^h S\, e^{-\int_0^h k_s X\, dh} \sec \phi\, dh \qquad (4)$$

where m is the ozone mass (in cm) in a vertical column. From Reference 20, the molecular scattering coefficient k_s is given by

$$k_s = \frac{32 \pi^3 M (n-1)^2}{3 N \rho \lambda^4} \qquad (5)$$

where M is the molecular weight of air, N is Avogadro's number, ρ is the air density, n is the index of refraction, and λ is the wave length. Also from Reference 20, the scattering function S is

$$S = \frac{2\pi^2 M (n-1)^2}{N \rho \lambda^4} \qquad (6)$$

From the Lorenz-Lorentz relation (Ref. 21):

$$\frac{n^2 - 1}{n^2 + 2} \frac{1}{\rho} = c \qquad (7)$$

where c is a constant. We note that for n close to 1, Equation (7) may be written

$$\frac{2}{3} \frac{n-1}{\rho} = c \qquad (8)$$

Substituting sea-level values of $n = 1.00028$ and $\rho = 1.25 \times 10^{-3}$ gm cm^{-3}, obtained from Reference 21, and solving for the constant we find $c \approx 0.15$, whence

$$\frac{n-1}{\rho} \approx 0.05\rho \qquad (9)$$

Hence both k_s and S are a function only of ρ

$$k_s = c_1 \rho \qquad (10)$$

$$S = c_2 \rho$$

where for $\lambda_1 = 0.311\mu$

$$c_1 = 8.6 \times 10^{-4} \text{ cm}^2 \text{ g}^{-1} \qquad (11)$$

$$c_2 = 5.2 \times 10^{-5} \text{ cm}^2 \text{ g}^{-1}$$

and for $\lambda_2 = 0.329\mu$

$$c'_1 = 6.8 \times 10^{-4} \text{ cm}^2 \text{ g}^{-1} \qquad (12)$$

$$c'_2 = 4.1 \times 10^{-5} \text{ cm}^2 \text{ g}^{-1}$$

Note that the ratio c_2/c_1 is $\frac{3}{16\pi} \approx .06$ regardless of wave length.

Substituting Equation (10) in Equation (4) and using the hydrostatic relation, we may integrate with the result:

$$\frac{I_\lambda}{I_{o\lambda} \sec\phi} = e^{-k_a m X} \frac{c_2}{c_1 X} \left(1 - e^{-\frac{c_1 X p}{g}}\right) \qquad (13)$$

where p is the pressure.

Substituting Equations (11) and (12) into Equation (13) we find

$$\frac{I_\lambda}{I_{o\lambda}} = 0.06 \frac{\sec\phi \, e^{-k_a m X}}{\sec 0 + \sec\phi} \left(1 - e^{-\frac{c_1 X p}{g}}\right) \qquad (14)$$

The ratio of intensities at wave length 1 to that of wave length 2 is then given by

$$\frac{I_{\lambda_1}}{I_{\lambda_2}} = \frac{I_{o\lambda_1}}{I_{o\lambda_2}} \frac{e^{-k_{a_1} m X}}{e^{-k_{a_2} m X}} \frac{\left(1 - e^{-\frac{c_1 X p}{g}}\right)}{\left(1 - e^{-\frac{c_1' X p}{g}}\right)} \qquad (15)$$

Since $I_{o\lambda_1}$ and $I_{o\lambda_2}$ are known, if I_{λ_1} and I_{λ_2} can be measured, then an estimate of the mass m of ozone may be made.

4.1.3 Calculations

For reasonable values of p, θ, and ϕ the ratio of the expressions in the parentheses of Equation (15) varies from about 1.1 to 1.2. The ratio $I_{o\lambda_1}/I_{o\lambda_2}$ for an 0.01μ wave length interval is about 0.67. Hence, without the ozone absorption factor, the ratio given by Equation (15) is about 0.8.

Let us define the principal factor as

$$\psi = \frac{e^{-k_{a_1} m X}}{e^{-k_{a_2} m X}} \qquad (16)$$

According to the Handbook of Geophysics (Ref. 22) for temperatures of 18°C and -44°C, K_{a_1} varies from 2.42 to 2.20 and k_{a_2} from .140 to .08. Using mean values of 3.2 and 0.11, the factor ψ is shown in Table 1 for various values of m X:

TABLE 1

RELATIVE SCATTERING OF 0.311μ TO 0.329μ RADIATION

m X (cm)	0.2	0.4	0.6	0.8	1.0	2.0
ψ	0.64	0.42	0.27	0.175	0.11	0.012

Plots of the ratio $I_{\lambda_1}/I_{\lambda_2}$ versus m for X = 2.0, 2.5, 5.0 and 10.0 have been derived from Table 1 and are shown in Figure 7. The value of X depends on both the zenith angle of the solar radiation, θ, and the zenith angle of the satellite sensor, ϕ. For θ and ϕ moderately small the value of X is very nearly 2, so that the plot for X = 2 of Figure 7 will apply in most cases. Should larger zenith angles be involved, values of X may be obtained from Figure 8.

It is seen from Figure 7 that the value of $I_{\lambda_1}/I_{\lambda_2}$ varies appreciably with the mass of ozone present in the atmosphere. Hence, the measurements of scattered solar radiation for the two wave lengths could be used to give an estimate of the total mass of ozone. Corrections would have to be made for the value of X if the zenith angles of either solar radiation or satellite sensor direction become large.

FIG.7 VARIATION OF RATIO OF SCATTERED RADIATION AT 311μ TO THAT AT .329μ VS TOTAL MASS OF OZONE IN THE ATMOSPHERE

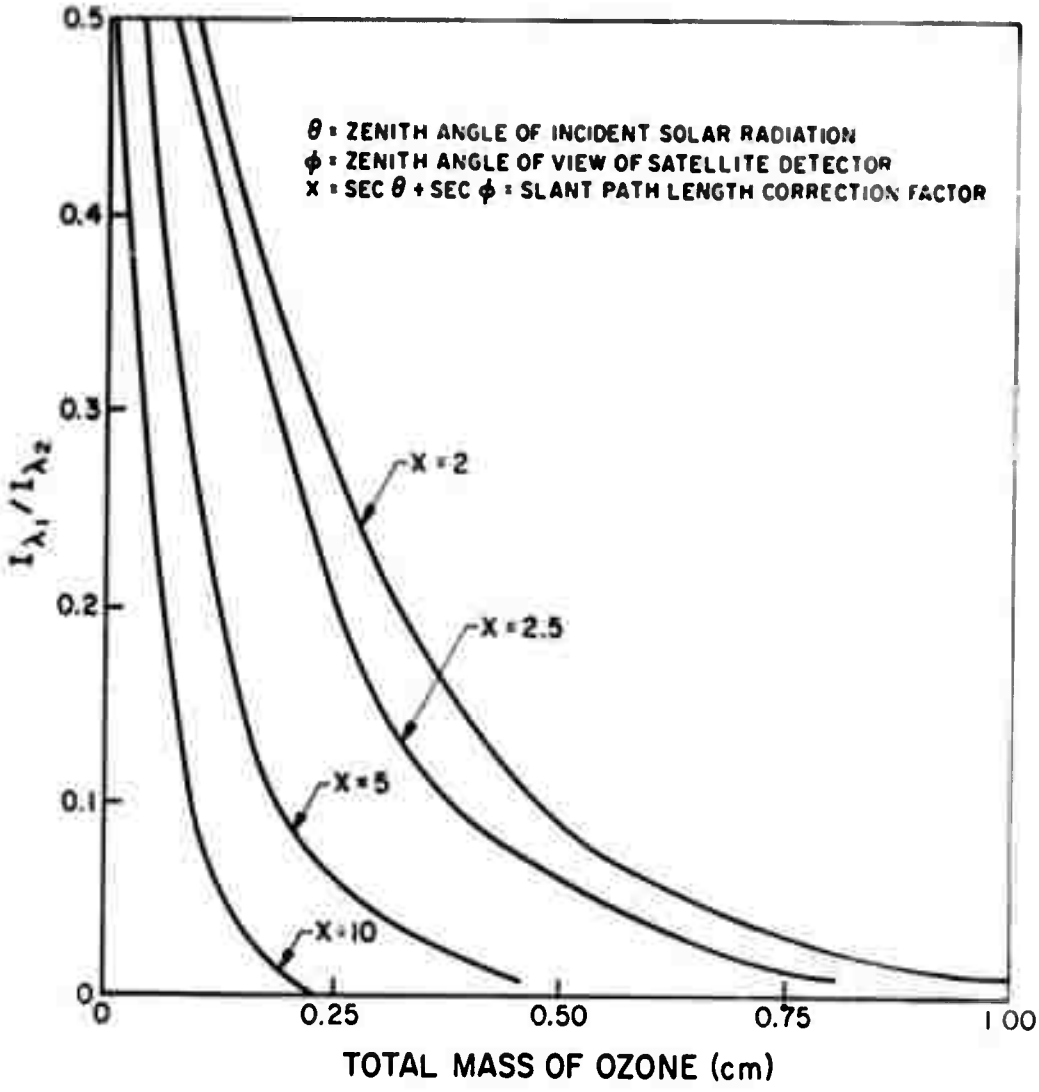

FIG.8 SLANT PATH LENGTH CORRECTION FACTOR (X)

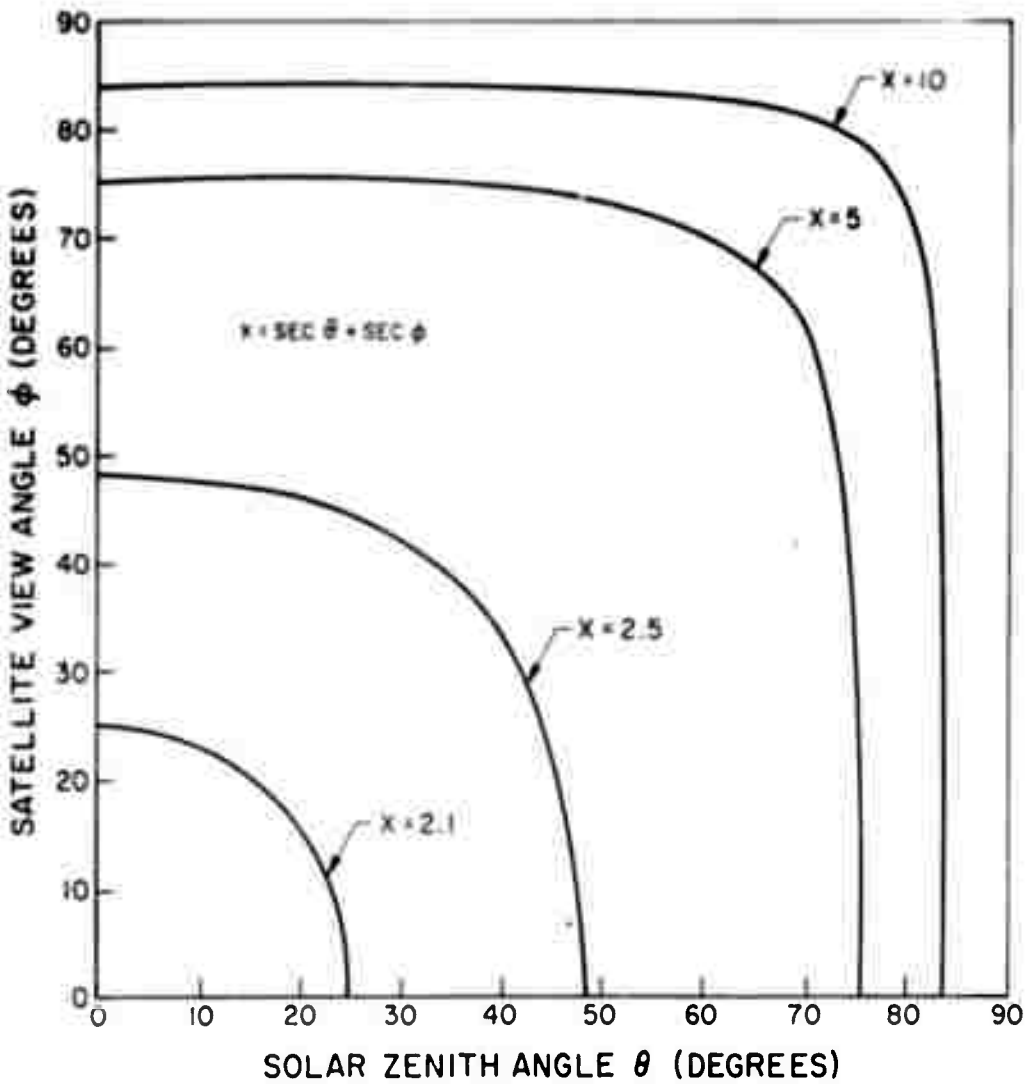

4.1.4 Discussion

The total ozone amount, or a number closely related to it, apparently can be determined by a measurement of relative absorption of scattered ultraviolet light. There are some complications that must be considered, however.

The back-scattering does not necessarily follow the Rayleigh law, particularly if the possibility of cloud scattering enters. Thus, a further group of observations is necessary to establish the "law" of scattering and the intensity of scattering. Since ozone absorption would occur at at least some of the wave lengths used to establish the scattering "law", rather complex equation-solving methods would be required.

Even with such additional complexities, it would seem that a well-designed satellite system could provide an excellent tool for the determination of the global distribution of total ozone.

4.2 A Preliminary Investigation of the Nature of the Infrared View of the Earth's Atmosphere from a Satellite*

4.2.1 Introduction

One proposed use of the satellite for meteorological purposes is to scan the atmosphere at an infrared wave length in which water strongly absorbs and emits. The varying intensity of radiation at this wave length would give an indication of the temperature at which the emission is taking place and of a part of the total heat balance. A preliminary investigation was executed to find the nature of the view that might be obtained from a scanning device that would create pictures as seen by infrared light. The present discussion will be limited to water vapor emission.

For the sake of simplification, it will be taken that the atmosphere is viewed at a wave length such that the water vapor is quite opaque. Such wave lengths are found in the 6.3μ band. It may be found more convenient to use wave lengths somewhat longer than this, say 7.5μ, in order to take advantage of the greater water-vapor emission which occurs near the peak of the black-body radiation. Differing choices of wave length also affect the region of the atmosphere from which most of the radiation will be emitted as will become apparent later.

---

* This research was conducted by Allied Research Associates, Inc. in part under Contract No. AF 19(604)-3881.

The view of the atmosphere as seen in an intense emission (and absorption) band of water will be that of a glowing fog. The intensity of glow will be related to the temperature of the top layer of the visible fog. The outer layers of the fog are somewhat transparent and, in general, the inside of the fog will be of a higher temperature than the outside. This presents a problem in the calculation of radiative transfer familiar to astrophysicists. A simplified approach yielding approximate numerical results will be presented here to demonstrate the behavior of the radiation. A heuristic approach is then adopted to investigate the meteorological significance of the radiation. Finally, a discussion of some applications is presented.

4.2.2 Radiation Source in the Atmosphere

4.2.2.1 Background

The intensity of radiation emitted normally from the top of an absorbing medium can be written

$$I_\lambda = \int_0^\infty K_\lambda B_\lambda (T)\, e^{-\tau_\lambda}\, ds \quad (\text{erg cm}^{-2}\ \text{sec}^{-1}\ \text{sterad}^{-1}\ \text{micron}^{-1}) \qquad (17)$$

where K_λ = absorption coefficient per length L, where the length ds in the atmosphere is measured in the same units as L. Calculations are often made in terms of K'_λ, the absorption coefficient per cm of water vapor, and w, the water content in cm of water vapor per length L of the atmosphere. In this notation, $K_\lambda = K'_\lambda w$.

$$\pi B_\lambda (T) = \frac{2\pi hc^2}{\lambda^5} \left(\frac{e^{hc}}{\tau kT} - 1 \right)^{-1} \quad \text{is the Planck function.} \qquad (18)$$

$$\tau_\lambda = \int K_\lambda\, ds \quad \text{is the optical depth.} \qquad (19)$$

By choosing different wave lengths in the micron range, one will effectively see different levels of the atmosphere, since the absorption coefficient ranges over a factor of about one thousand in going from the depths of the water-vapor band at 6.5μ to the "window" near 11μ. For simplicity, it is advisable to choose regions of the spectrum which have only water vapor bands present (avoid O_3, CO_2, etc. bands).

In order to observe high levels in the atmosphere (to avoid confusion with the ground) the calculations here concentrate on the wave length regions where the water vapor absorption is large – e. g. in the range K'_λ = 30 to 300 cm^{-1} of water vapor at S. T. P.

4. 2. 2. 2 Calculations

All quantities and calculations here are approximate. The parameters of the atmosphere on January 19, 1954 were obtained from the measurement of Murgatroyd et. al. (Ref. 23); these parameters are the pressure, temperature and water content as a function of height and appear in Table 2.

Now the absorption coefficient K'_λ is a function of temperature and pressure; here only the pressure dependence is approximately included by setting $K'_\lambda = (p/p_s)\, k_\lambda$, where k_λ is the absorption coefficient per cm of water vapor measured in the laboratory at pressure p_s, and p is the ambient pressure. While there is some question about the form of the pressure dependence, Kaplan (Ref. 24) and Taylor and Yates (Ref. 25) have been followed in assuming the absorptivity is directly proportional to pressure.

To integrate Equation (17), the atmosphere is divided into 2000 foot elements of height and the change in optical depth in each is then approximately given by:

$$\Delta \tau_\lambda \text{ (2000 ft)} = \frac{p}{p_s} \; k_\lambda \; w \qquad (20)$$

where k_λ is in cm^{-1} and w is in cm of H_2O per 2000 ft of atmosphere at the particular level considered.

Rewriting Equation (17) as

$$I_\lambda = k_\lambda \int_0^\infty \left[\frac{\Delta \tau_\lambda}{k_\lambda} \; B_\lambda (T) \right] e^{-\tau_\lambda} \, ds \qquad (21)$$

with ds in units of 2000 ft, the quantity $\Delta \tau_\lambda \, B_\lambda / k_\lambda$ can be tabulated as a function of height (independent of k_λ).

Calculations for k_λ = 300, 30, 3 cm^{-1} of water vapor are given in Table 2. Bacause of the relative flatness of the black-body radiation curve in this region, a value of $\lambda = 6.75\mu$ was used to compute B_λ for each k_λ. Note also that τ_λ / k_λ for any height is obtained by adding together the tabulated values of $\Delta \tau_\lambda / k_\lambda$ for all higher levels.

TABLE 2

PARAMETERS OF ATMOSPHERE OF JANUARY 19, 1954 AND CALCULATIONS OF RADIATION INTENSITY FOR VARIOUS ABSORPTION COEFFICIENTS

h (1000 ft)	T (°C)	$\frac{p}{p_s}$	H_2O (cm/1000 ft)	$\frac{(\Delta\tau_\lambda)\,\pi B_\lambda}{2.7\times10^7 k_\lambda}$	$\frac{\tau_\lambda}{k_\lambda}$	$e^{-\tau_\lambda}$			Integrand = $\frac{(\Delta\tau_\lambda)\,\pi B_\lambda\, e^{-\tau_\lambda}}{2.7\times10^7 k_\lambda}$		
						$k_\lambda = 300$	30	3	300	30	3
30	-45	0.30	0.0005	3×10^{-8}	0.0003	.91	.91	.99	28×10^{-9}	3×10^{-8}	0×10^{-7}
28	-39	0.33	0.0006	5.4	0.0007	.85	.98	.99	46	5	1
26	-34	0.36	0.0009	10.0	0.0014	.66	.96	.99	66	10	1
24	-28	0.39	0.0012	18.2	0.0023	.50	.93	.99	92	17	2
22	-23	0.43	0.0017	26	0.0038	.32	.89	.99	116	32	4
20	-19	0.47	0.0038	98	0.0074	.109	.80	.98	108	78	10
18	-15	0.50	0.0076	234	0.0150	.0111	.64	.96	26	148	22
16	-10	0.54	0.014	540	0.0302	.00012	.41	.92	1×10^{-9}	220	50
14	-6	0.60	0.027	1280	0.062		.156	.89		200	114
12	-3	0.65	0.048	2720	0.125		.0235	.69		64	186
10	+1	0.70	0.08	5240×10^{-8}	0.24		.00075	.59		4×10^{-8}	316×10^{-7}

To find the intensity at the satellite, assume that its height h above the ground is much greater than the height of any water vapor which contributes appreciably to the intensity. Let A be the area of atmosphere from which radiation is received and $\Delta\lambda_\mu$ be the width of the filter in microns. Then the energy in this band received at this satellite is

$$E_\lambda (\Delta\lambda_\mu) = \frac{A\,\Delta\lambda_\mu}{4\pi h_s^2} I_\lambda \text{ (erg cm}^{-2}\text{ sec}^{-1}\text{)} \qquad (22)$$

For A = 10,000 km^2 and a receiving area of 1000 cm^2, and h_s = 200 km, the energy received is

$4.1 \times 10^4\ \Delta\lambda_\mu$ erg sec^{-1} for k_λ = 300 cm^{-1} ($4.1\ \Delta\lambda_\mu$ mw)

$2.2 \times 10^4\ \Delta\lambda_\mu$ erg sec^{-1} for k_λ = 30 cm^{-1} ($2.2\ \Delta\lambda_\mu$ mw)

For radiation in the region λ = 6.75μ, these represent about 10^{17} photons sec^{-1}.

From Table 2, part of which is plotted in Figure 9, it is seen that the major contribution to the integral (17), and, therefore, to the total intensity received at the satellite, comes from a slice of the atmosphere of small thickness. For example, the region 14,000 - 18,000 ft contributes about 70% of the intensity at k_λ = 30 cm^{-1}; the region 20,000 - 24,000 ft contributes about 60% at k_λ = 300 cm^{-1}.

4.2.3 An Heuristic Approach

4.2.3.1 Introduction

The results of the previous section indicate that the bulk of the radiation departing the outside of the atmosphere at any given wave length emanates from a relatively thin atmospheric stratum. We will now proceed to examine the meteorological significance of this localized source of the radiation. In the interests of lucidity of argument, a very approximate approach will be used, with specific numerical values chosen ad-lib for illustration. The objective will be to find the meteorological parameters that define the stratum from which the radiation originates.

FIG.9 CALCULATED DISTRIBUTION OF INTENSITY OF RADIATION FROM WATER VAPOR IN THE ATMOSPHERE OVER SOUTHERN ENGLAND, 19 JANUARY 1954

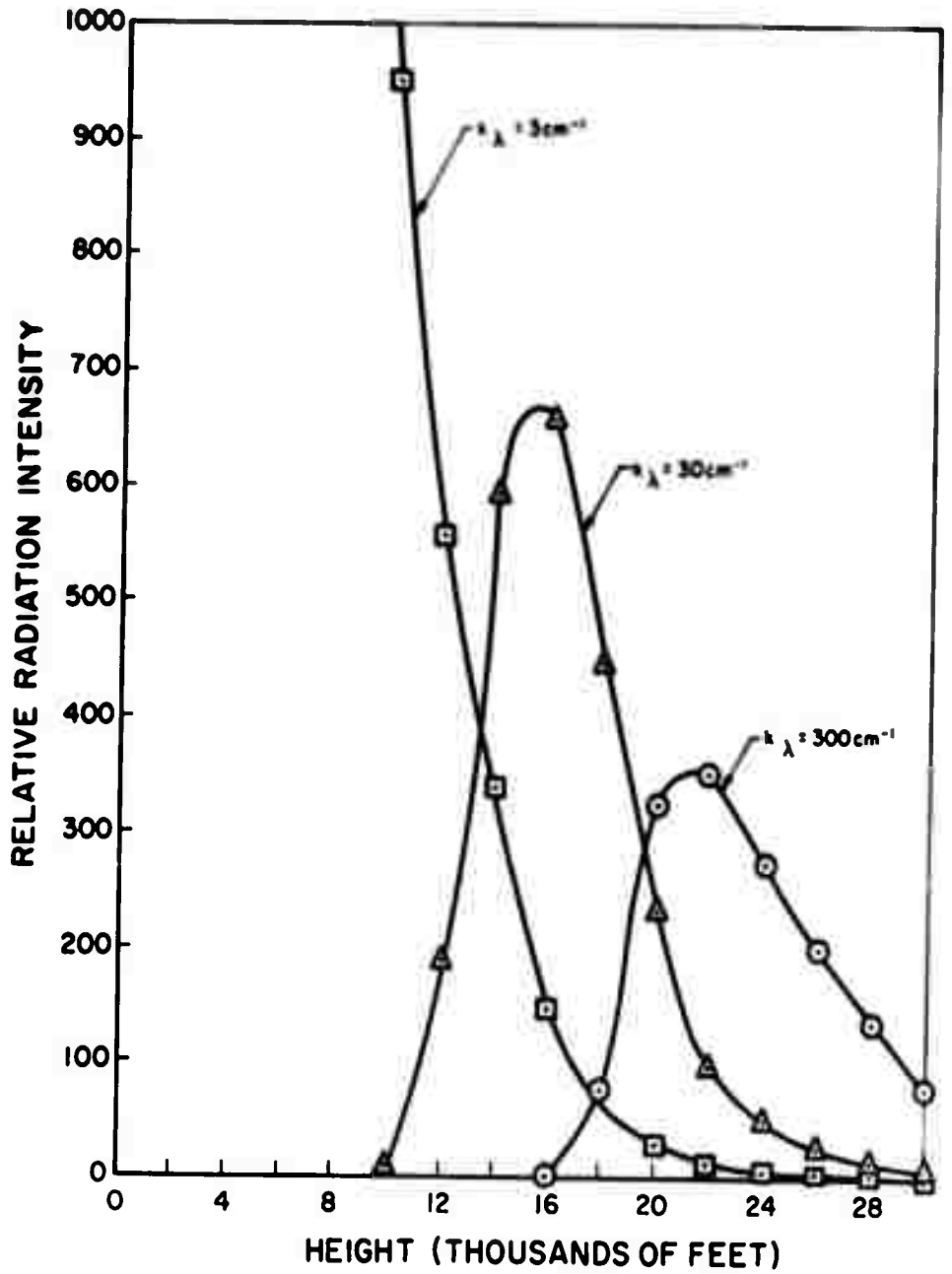

4.2.3.2 Background

Let us examine the path that the infrared must traverse on its way through the atmosphere to the satellite. The absorptivity of water vapor is greater at higher pressures than it is at lower, as a result of pressure broadening of lines. As in Section 4.2.2.2 we assume that the absorption coefficient is directly proportional to pressure. Standard absorptivity will be considered to occur at 1000 millibars.

The water equivalent path length is defined by

$$du = \frac{p}{1000} a dz \tag{23}$$

where u is the equivalent water path length in cm, p is the pressure in millibars, a is the absolute humidity or vapor density in gm cm^{-3}, z is the geometric path length in cm (here assumed to be in the vertical). Note that a is also the number of cm of water per cm of path length since the density of water is 1 gm cm^{-3}. Various hydrostatic and gas law substitutions may be made, resulting in such forms as

$$du = 6.4 \times 10^{-4} e dp \tag{24}$$

or

$$du = \frac{.0217\, pe}{T} dz \tag{25}$$

Here e is the vapor pressure in millibars, and T is the absolute temperature in degrees Kelvin.

Results of calculations of equivalent water path length from the top of the atmosphere (or rather, the top of the flight), taken from the data collected with a frost point hygrometer by Murgatroyd et. al. (Ref. 23) are shown in Figure 10. It is seen that the increase of equivalent water path length with depth going down through the atmosphere is roughly exponential. The slope is such that the increase of equivalent water path length in about 2000 feet of geometric path is about the same as the total equivalent water path length above the 2000 foot increment.

The same data plotted on a linear scale of path length is shown in Figure 11. It is seen that a sharp bend occurs in the curve, the position of the bending being dictated somewhat by the choice of the scale of plotting. This bend marks the altitude at which the absorption begins to increase

FIG.10 TOTAL EQUIVALENT WATER PATH LENGTH VS ALTITUDE IN THE ATMOSPHERE OVER SOUTHERN ENGLAND, 19 JANUARY 1954

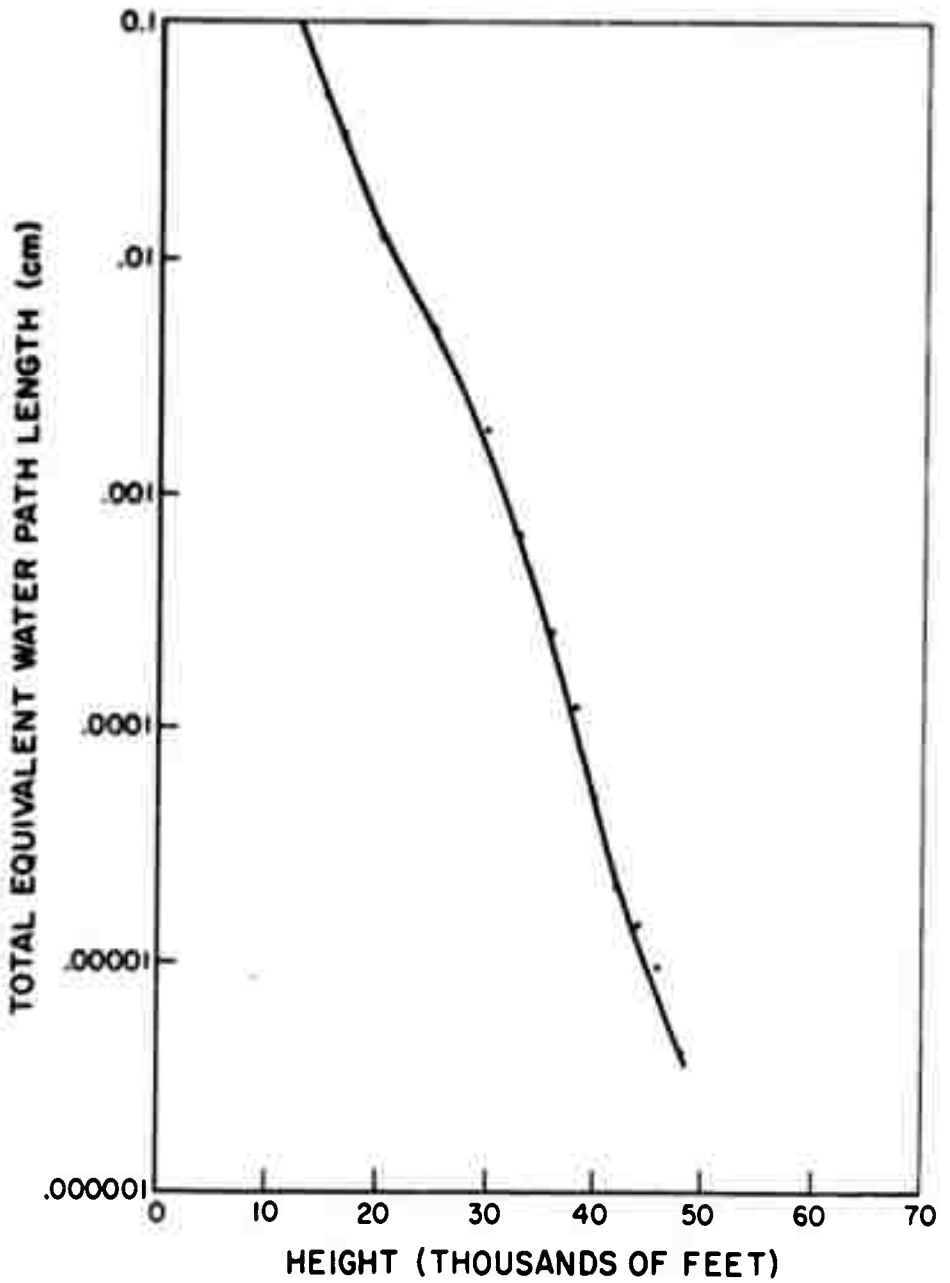

markedly. Noting that the bend occurs at about .05 cm path length, the view of the atmosphere at a wave length such that the absorption is essentially total in a .05 cm equivalent water path length will not penetrate appreciably below the corresponding altitude. Plotting dewpoint temperature vs. altitude on Figure 11, it is found that this path length corresponds to a dewpoint temperature of -30°C. In the present case, this corresponds to an air temperature of -9°C.

The water equivalent path in the 2000 feet immediately surrounding the -30°C dewpoint position is, as has been illustrated above, about the same as the total water equivalent path down to that point. Since the temperature at the -30°C dewpoint is materially higher than temperatures at higher elevations, the radiant intensity emanating from the -30°C region will be greater than that emanating from the regions above. Admittedly, part of the -30°C radiation will be absorbed on its way out, but this absorption will be in part replaced by radiation at a lower temperature from the reaches above. Essentially, then, the -30°C dewpoint marks the outside of the glowing fog, as seen at the appropriate wave length. A change in wave length would make possible the definition of another dewpoint temperature as the outside of the fog.

It remains to be demonstrated that the dewpoint temperature is an adequate description of the outside of the glowing fog. A scatter plot of dewpoint temperature against the rate of increase of path length with depth – i.e. corresponding to the slope - du/dh of the equivalent water path length curve of Figure 11 – taken from random samplings of radiosonde data over the North American continent from Alaska through Mexico and Central America is shown in Figure 12. The actual heights of the various iso-dewpoint surfaces varied considerably. It will be seen that there is very small scatter in the data, so that any dewpoint that may be chosen as characteristic of the outside of the glowing fog for a given wave length will represent a constant value of increase of optical depth wherever it is met.

The radiation from the constant dewpoint surface is a function of the temperature of that surface. As might be expected, the temperature range associated with a given dewpoint is not very large. The temperatures associated with the same data plotted in Figure 12 are shown in Figure 13.

FIG. 11 EQUIVALENT WATER PATH LENGTH AND DEW POINT TEMPERATURE vs ALTITUDE IN THE ATMOSPHERE OVER SOUTHERN ENGLAND, 19 JANUARY 1959

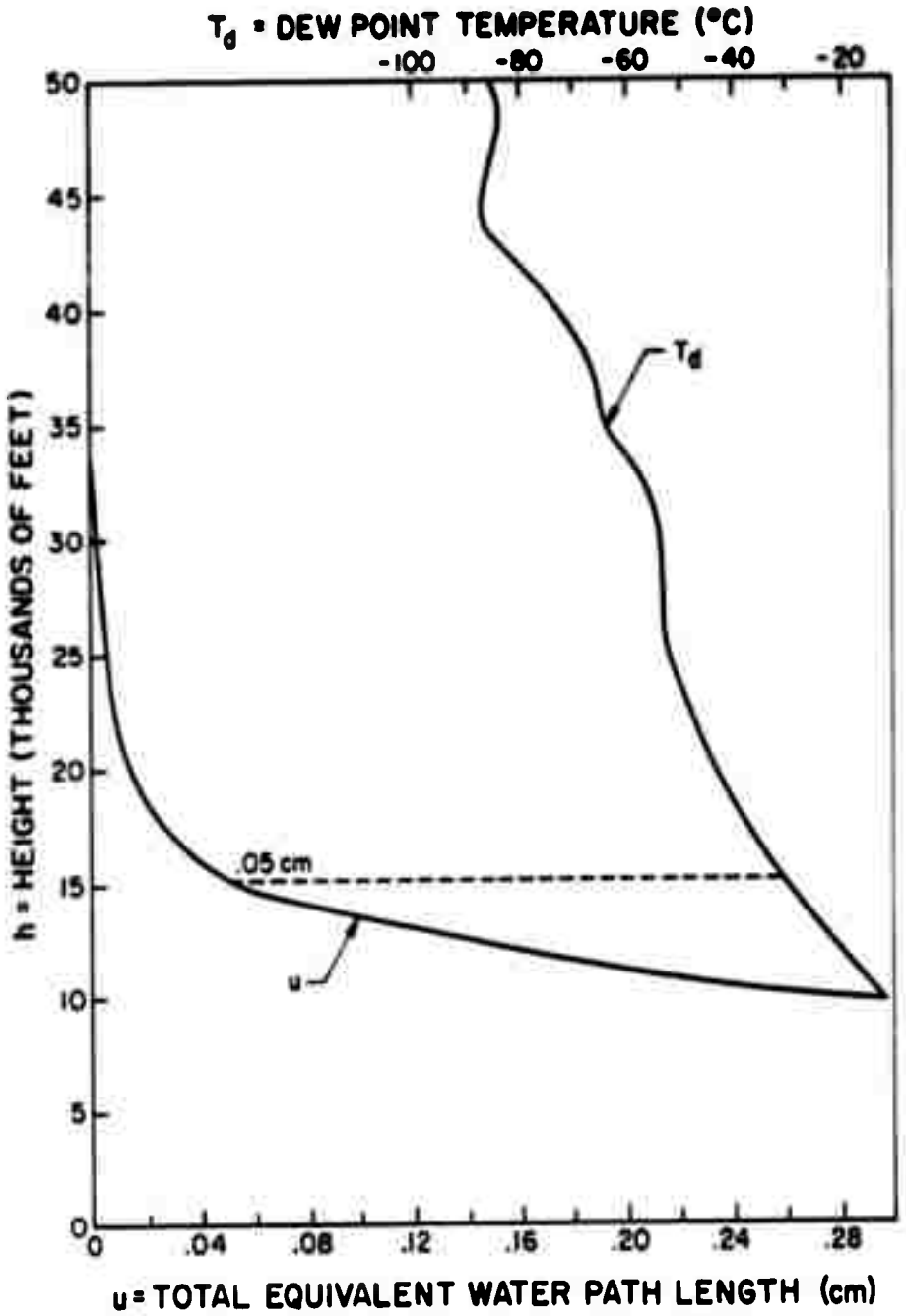

Fig. 12 OBSERVED RATE OF INCREASE OF EQUIVALENT WATER PATH LENGTH WITH DEPTH vs DEW POINT TEMPERATURE

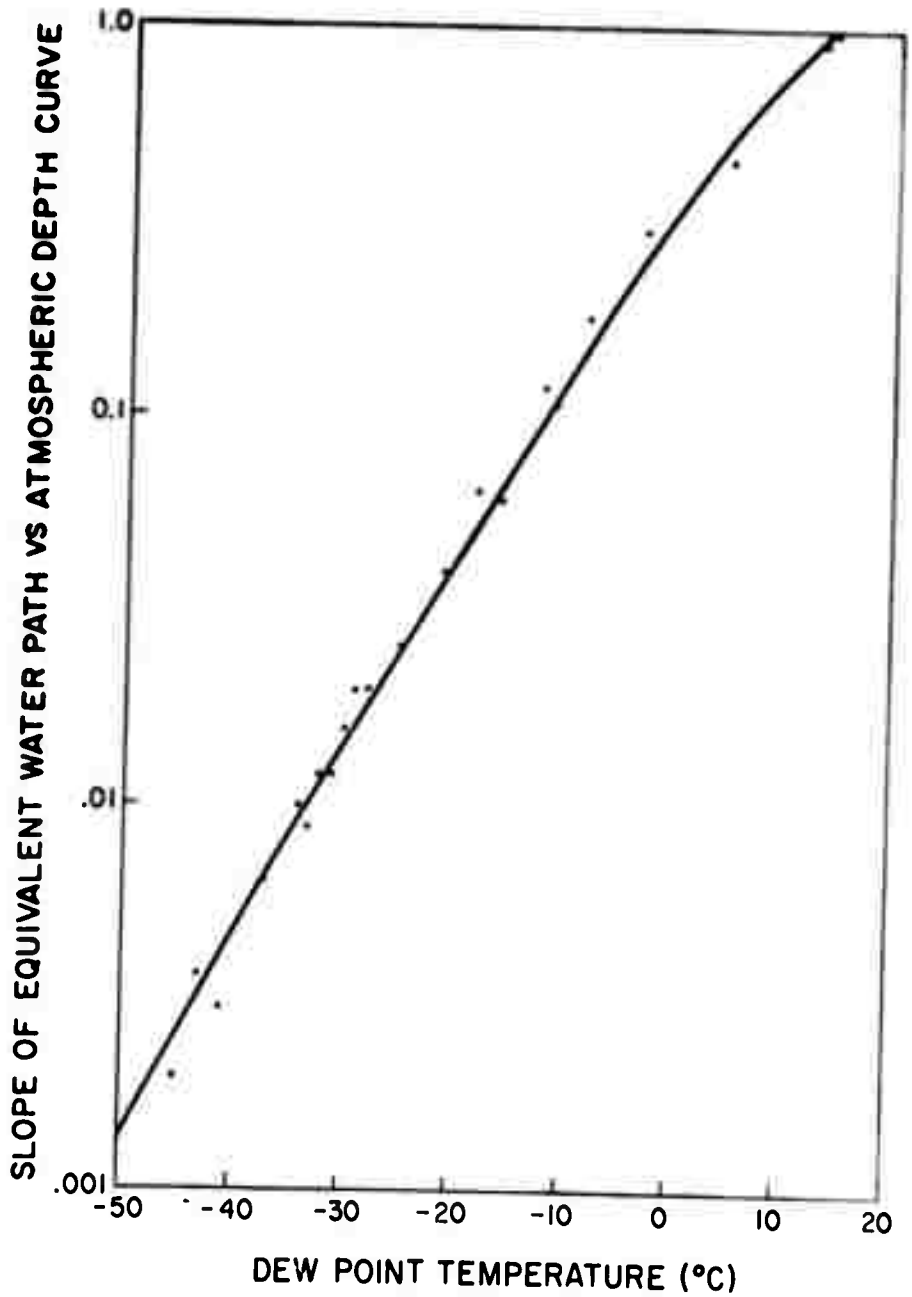

FIG. 13 OBSERVED RATE OF INCREASE OF EQUIVALENT WATER PATH LENGTH WITH DEPTH vs TEMPERATURE CORRESPONDING TO DATA OF FIGURE 12

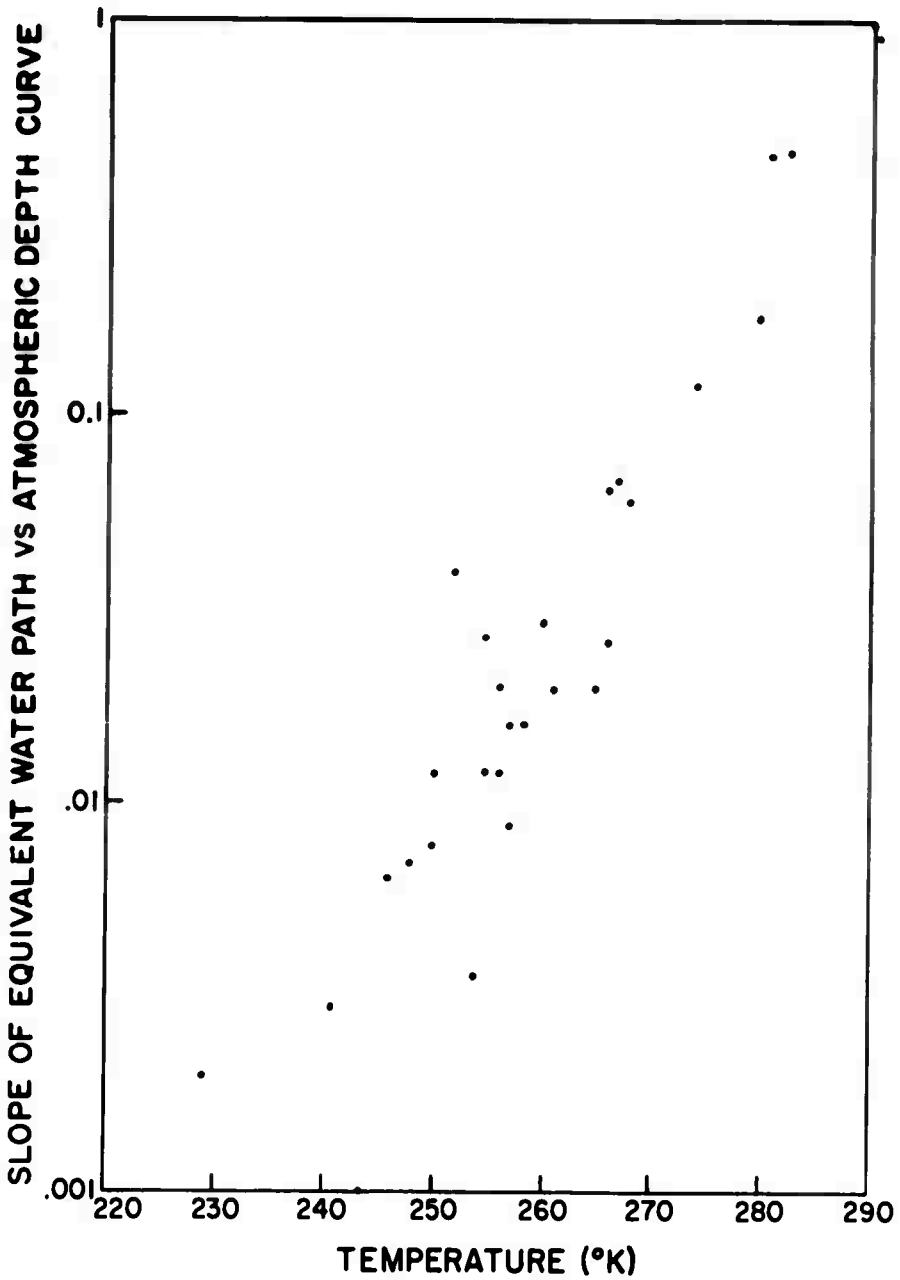

The spread of temperatures is somewhat greater than that of dewpoints, having a maximum scatter in the 240°K to 270°K region corresponding to dewpoints of the order of -40°C to -10°C. Results of a statistical tabulation of the temperature associated with the -30°C dewpoint from radiosonde reports over the North American continent on a single day are shown in Figure 14. The curve has a mode at about -16.3°C, a mean at -19.4°C, and a standard deviation of 4.6°C. (The mode was determined by fitting a parabola to the points at -20°C, -17°C, and -14°C). It is seen that the range of temperatures associated with a given dewpoint, and thereby the outside of the glowing fog, is not very great.

It may be more instructive to cast these data over to the amount of radiation corresponding to the temperatures of the atmosphere at the -30°C dewpoint. The result of this transformation is shown in Figure 15. Radiation amounts and number of cases are now shown in arbitrary units, avoiding the need to normalize. The curve has a fairly sharp mode, and the standard deviation is found to be only 15% of the value of the mean. (In arbitrary units, the mean is at 11.8 and the standard deviation is 1.77.) The total spread of radiation covers about a 2 to 1 ratio.

This apparently indicates that a relatively limited amount of variation will be found in the radiation emerging from the glowing fog at the strong emission bands. The amount of emission will not depend of itself on the height in the atmosphere at which the water "ends", but rather on the relative humidity at the -30°C (or other appropriate to the wave length) dewpoint temperature. While the meteorological significance of this quantity is not immediately apparent, it will be seen in the next section to have some interesting properties.

4.2.4 Synoptic Behavior of Water Vapor Infrared Emission

4.2.4.1 Introduction

Sections 4.2.2 and 4.2.3 point out that the vast bulk of the emission in the dense sections of the water vapor emission bands emanates from relatively thin strata of the atmosphere. It was shown that these strata are characterized by being surfaces of essentially constant dewpoint. The

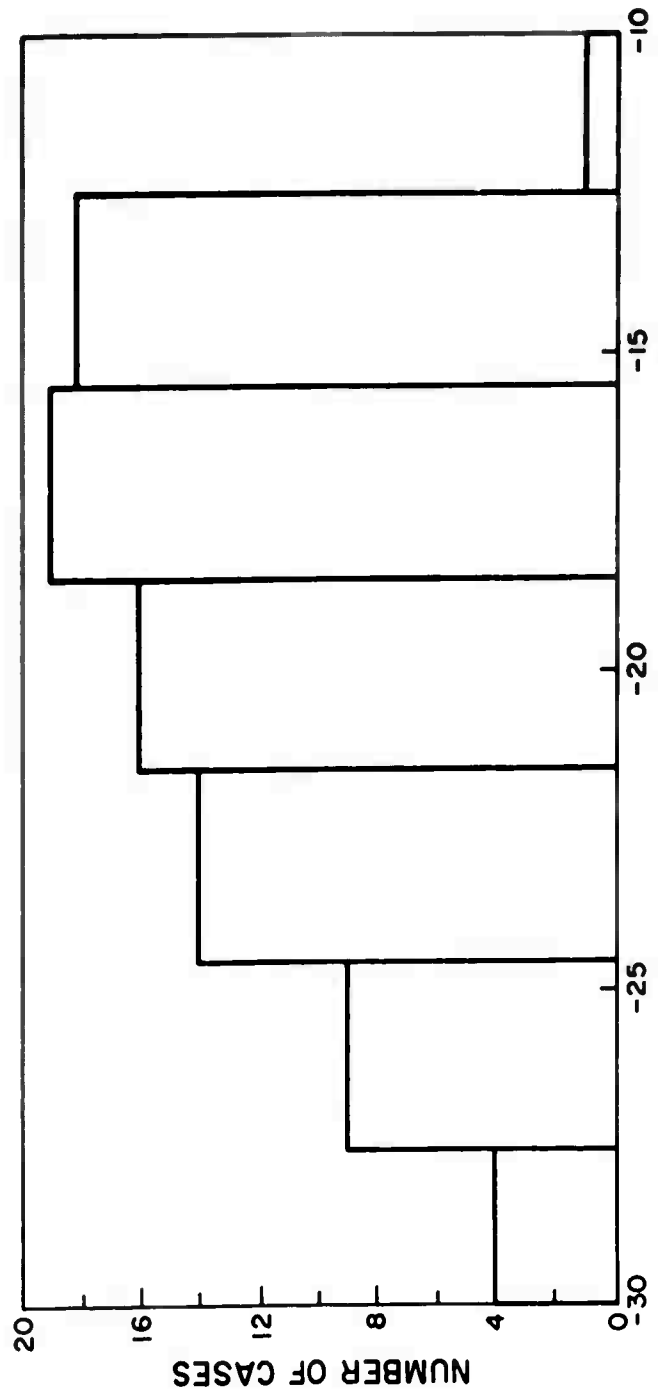

FIG. 14 DISTRIBUTION OF TEMPERATURE ASSOCIATED WITH THE -30°C DEW POINT

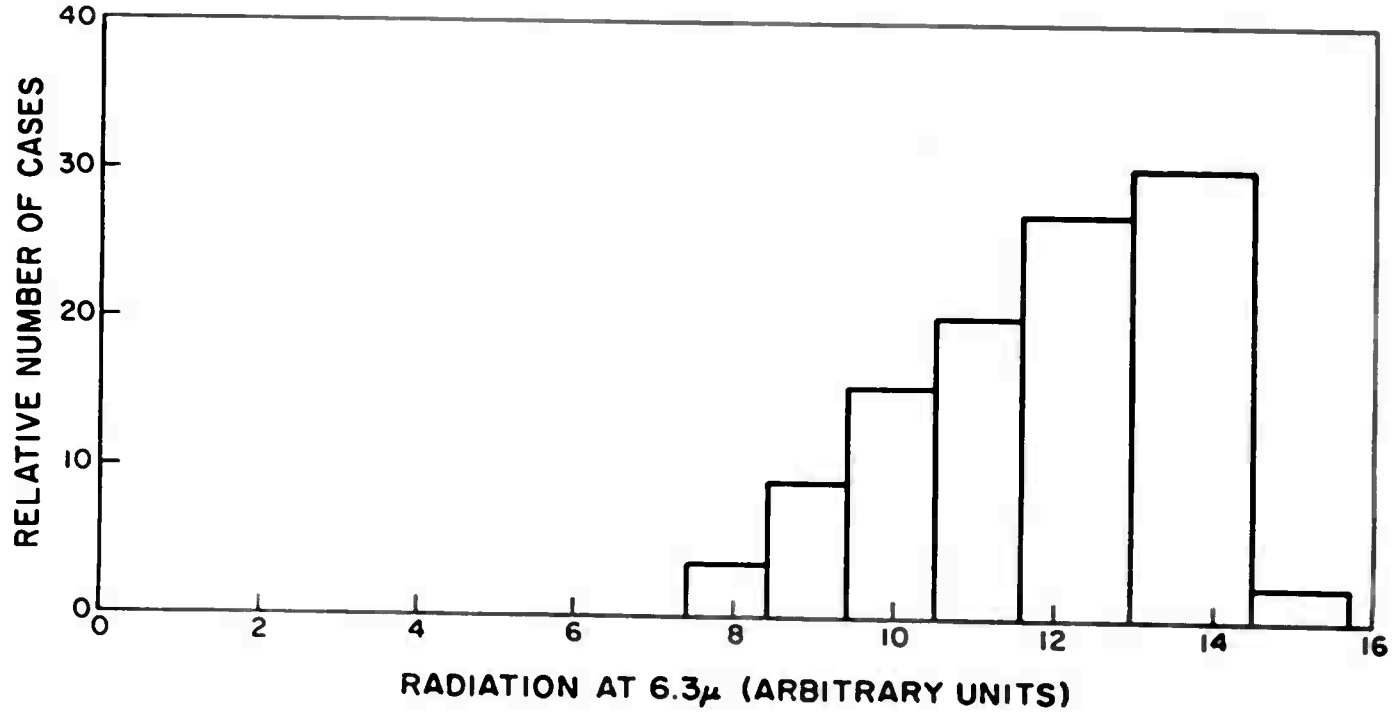

FIG 15 DISTRIBUTION OF RADIATION ASSOCIATED WITH THE -30°C DEW POINT

amount of emanation is controlled by the temperature of this constant dewpoint surface. In this section, an attempt will be made to develop the synoptic significance of the temperature of a constant dewpoint surface.

Synoptic charts of the temperature of constant dewpoint surfaces were prepared for successive days. The period was chosen essentially at random and two surfaces were used, the zero degree dewpoint and the -20°C dewpoint surface. Isotherms have been drawn upon these surfaces, a 4°C interval being used as a matter of convenience. Analysis was performed by personnel unfamiliar with the conventional weather map analyses of those days.

Two difficulties attended the preparation of these charts from radiosonde data. In warm areas – ie., areas of great difference between the temperature and the dewpoint – it was frequently found that motor-boating was reported, making it difficult to assign rational temperatures. In other cases, it was found that the dewpoint surface intersected the ground, indicating that even the relatively small quantities of water vapor required for ground obscuration were not present. This latter hazard, of course, would also be present in real observations from a satellite.

4.2.4.2 26 April 1955, 0300 Z

The temperature map of the 0°C surface presented in Figure 16 shows interesting similarity to many of the features of the surface analysis for that day shown in Figure 17. The cold band extending from the Los Angeles region through Idaho toward the Dakotas corresponds reasonably well with the band of precipitation associated with the complex frontal system in the West. The warm tongue invading the southern Rocky Mountains is found to correspond quite well with the anticyclone in that region. A cold region is found to occupy the same area as the band of precipitation and cloudiness extending from northern New England to the northern Georgia region. The rather flat high between the Great Lakes and Louisiana is relatively poorly marked by a warm band. There is believed to be little reality to the cold stripe covering the Gulf and Caribbean Islands.

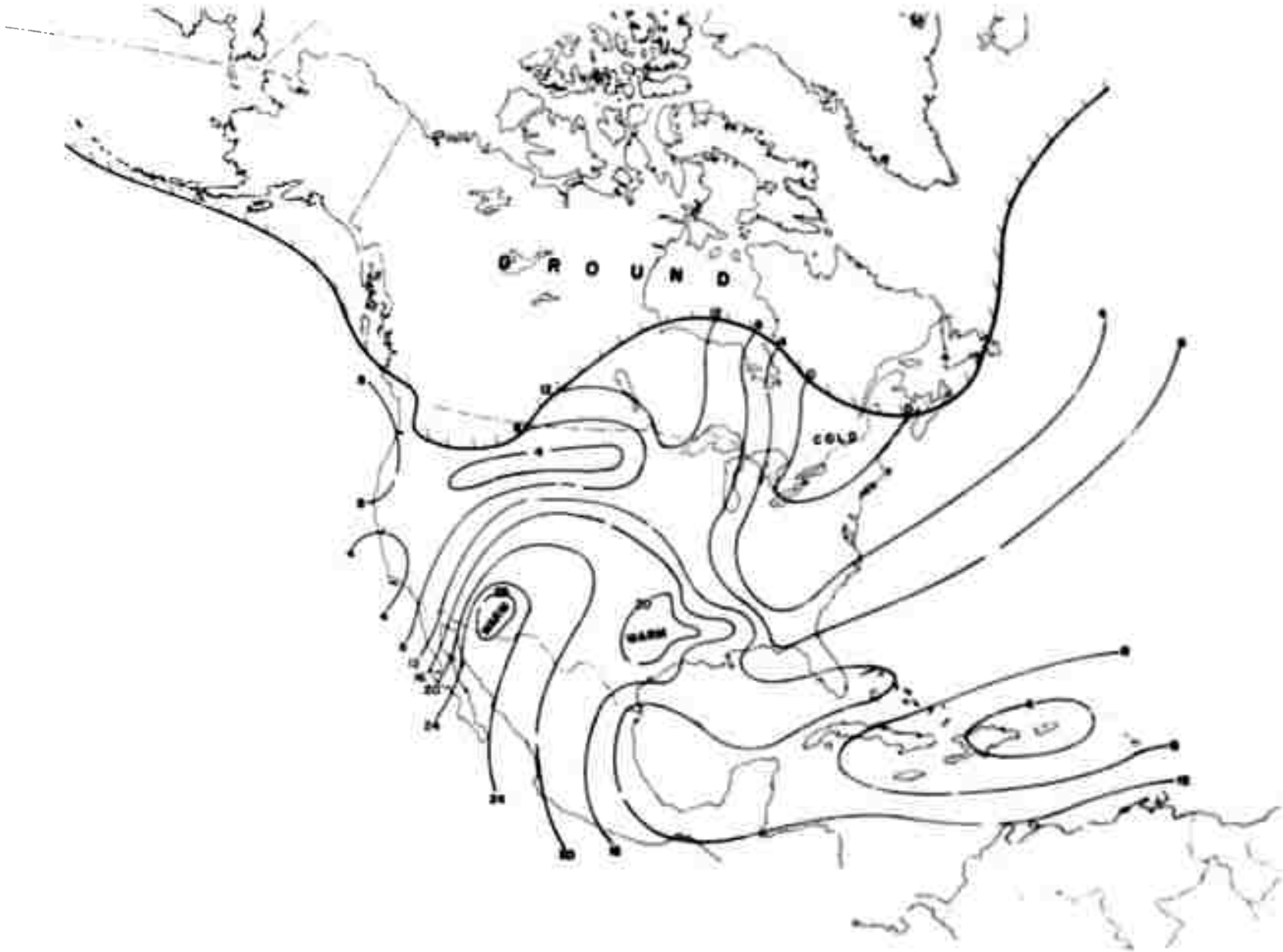

Fig. 16 0300Z, 26 APRIL 1955, TEMPERATURE AT 0° DEWPOINT SURFACE

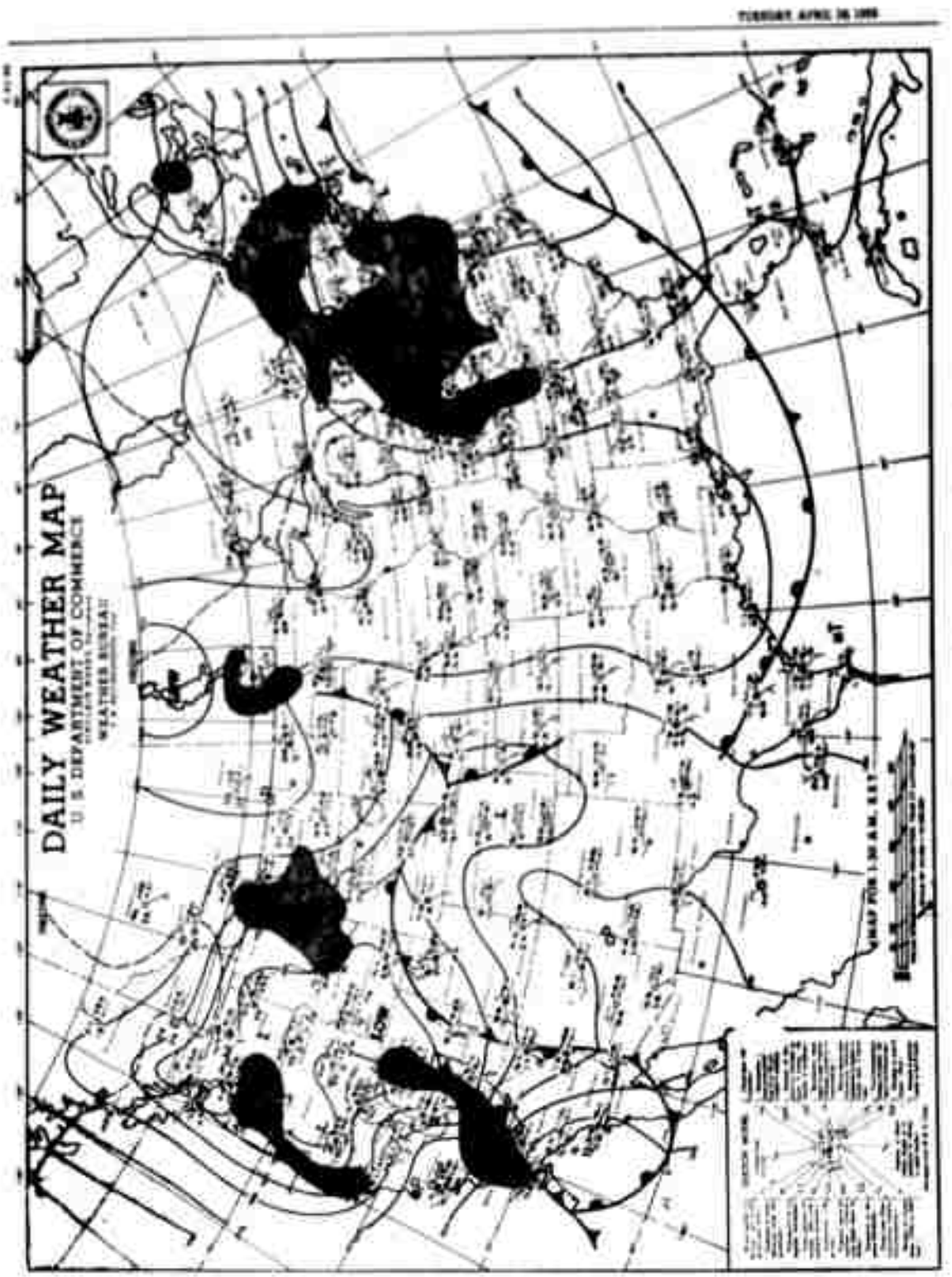

Fig. 17 SURFACE MAP, 0630Z, 26 APRIL 1955

At the -20° dewpoint surface shown in Figure 18, the pattern is less clearly marked. The principal cold band extends over the northern tier of states. On the Atlantic side separate cold centers appear to correspond to lows over Pennsylvania and off the New England coast, respectively. The warm tongue over the southern United States is now shifted eastward. Any correspondence of the band over the Gulf and Florida with the indicated cold front is probably fortuitous.

The upper air chart given in Figure 19 shows that the strong gradient of temperature on the constant dewpoint surface across the northern tier of states delineates on the position of the jet stream at 500 mb. It follows such features as the abrupt southward bend of the jet stream over the Great Lakes area and its curvature about the low over Pennsylvania.

The warm incursion in the southern part of the country is seen to correspond to the anticyclonic area observed there at 500 mb, and similarly, the warm pocket in British Columbia corresponds to a small wedge in that area. Since the delineation of this warm area depends essentially upon a single observation, it may be somewhat over-emphasized.

4.2.4.3 27 April 1955, 0300 Z

The 0° dewpoint map of Figure 20 has assumed a noticeable meridional nature in keeping with the development seen on the surface chart of Figure 21. The major significant features are a warm band now extending from the southwest to the Great Lakes and a cold band from New England down through the middle South. This corresponds to an observed band of cloudiness which does not correspond to any particular manifestation on the surface chart. Representation of the principal features of the cyclonic system in the West has been disrupted by insufficient quantities of water vapor in the mountain states.

On the -20° dewpoint surface shown in Figure 22, the central United States is dominated by a bifurcating warm tongue. While this bifurcation does not find any complete counterpart on the 500 mb chart of Figure 23, it is in fact a precursor of later developments. It does, in general, correspond to the expanding ridge in the Central States extending up through Canada toward Hudson Bay. Delineation of the jet stream by the gradient areas does not appear to be as good on this chart as previously. This is

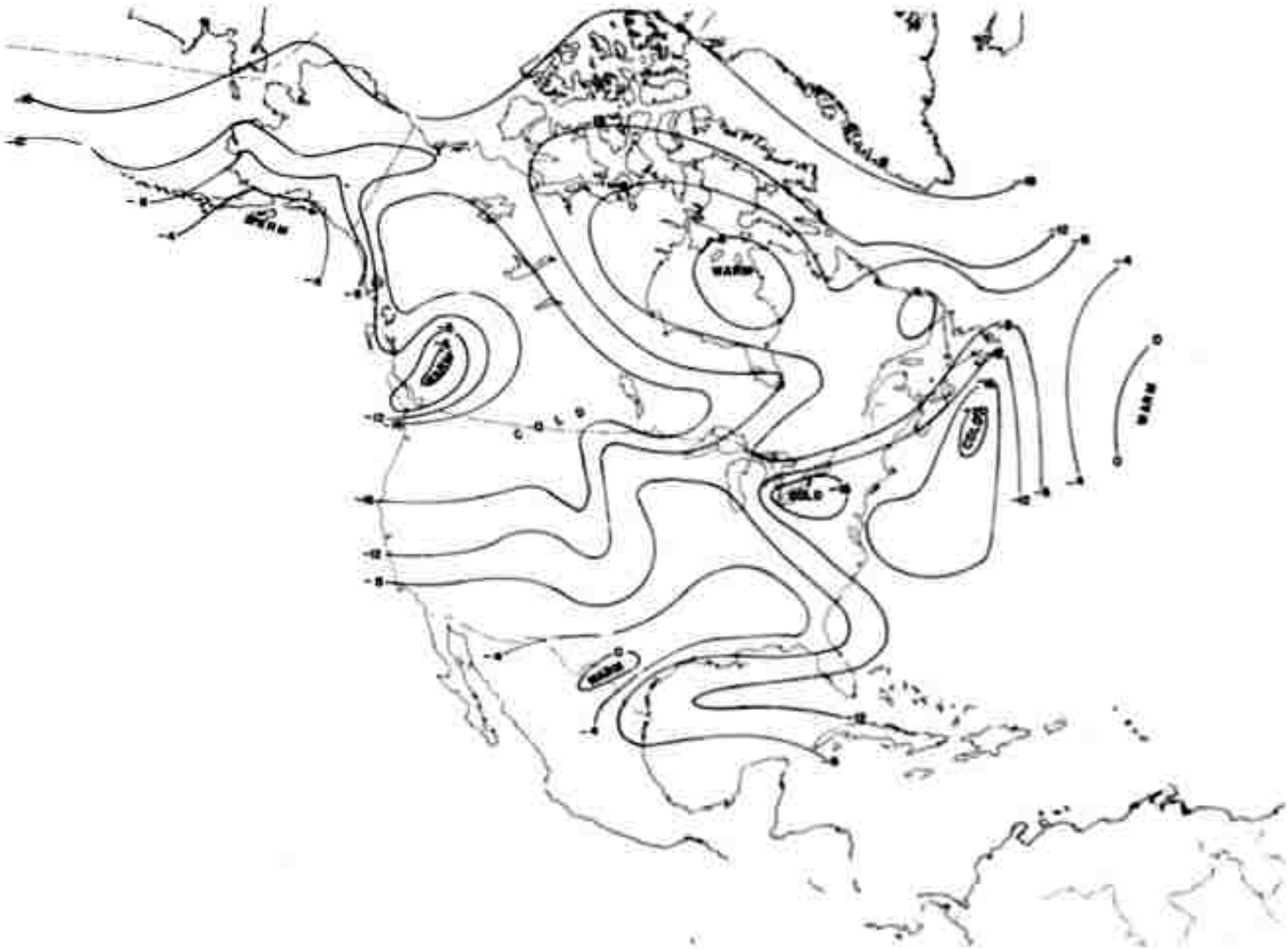

Fig. 18 0300Z, 26 APRIL 1955, TEMPERATURE AT -20° DEWPOINT SURFACE

Fig. 19 500 mb CHART, 26 APRIL 1955, 0300Z

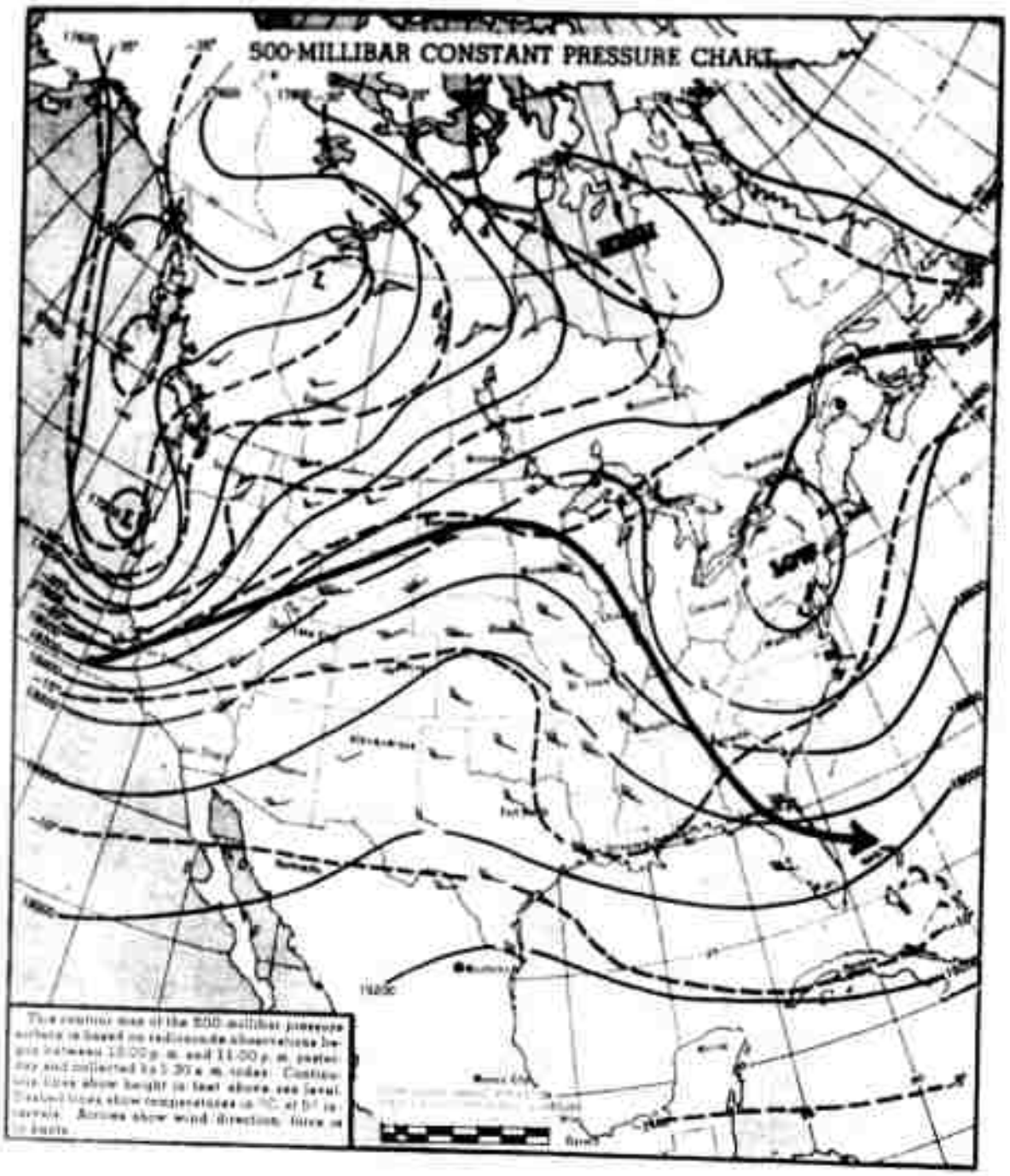

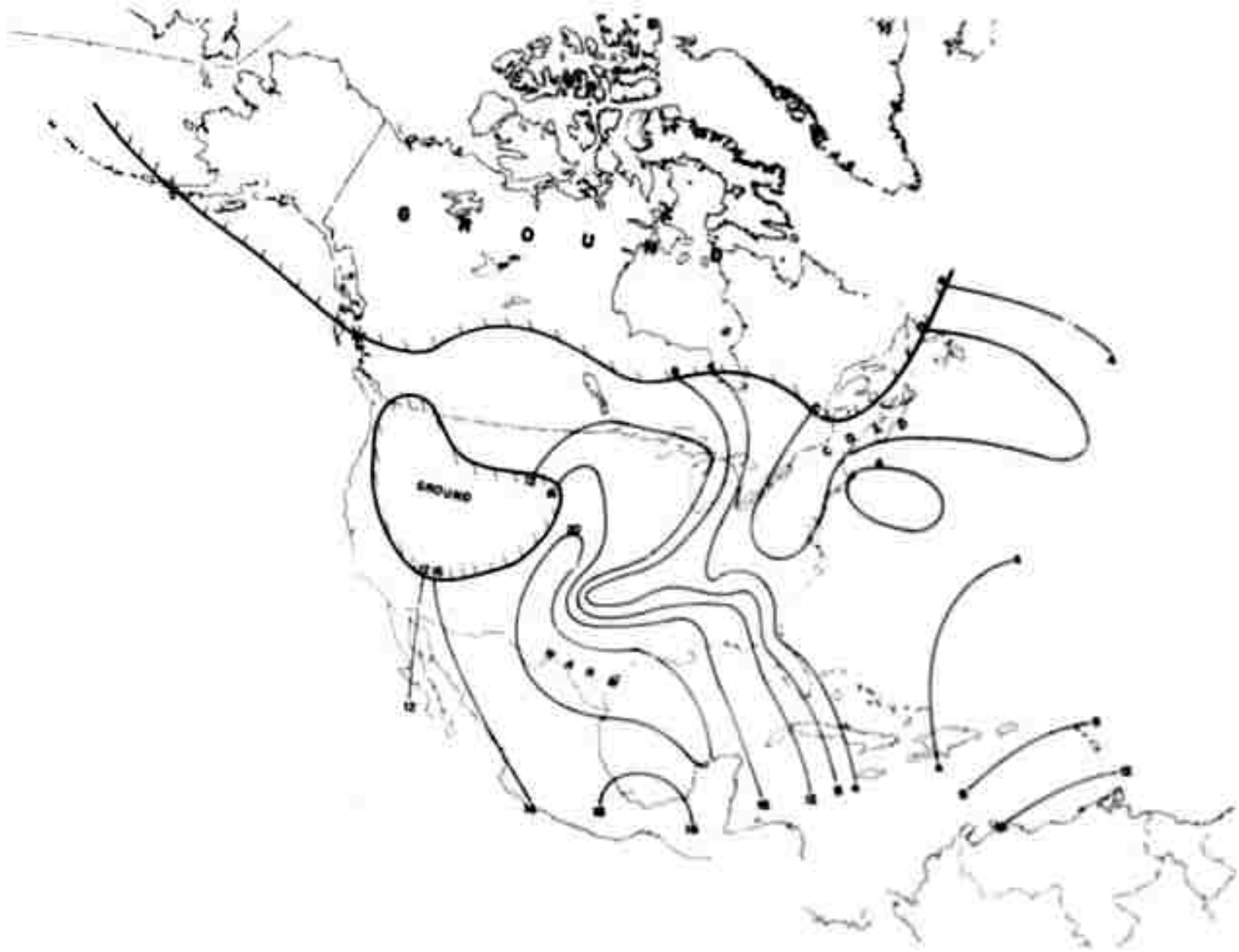

Fig. 20 0300Z, 27 APRIL 1955, TEMPERATURE AT 0° DEWPOINT SURFACE

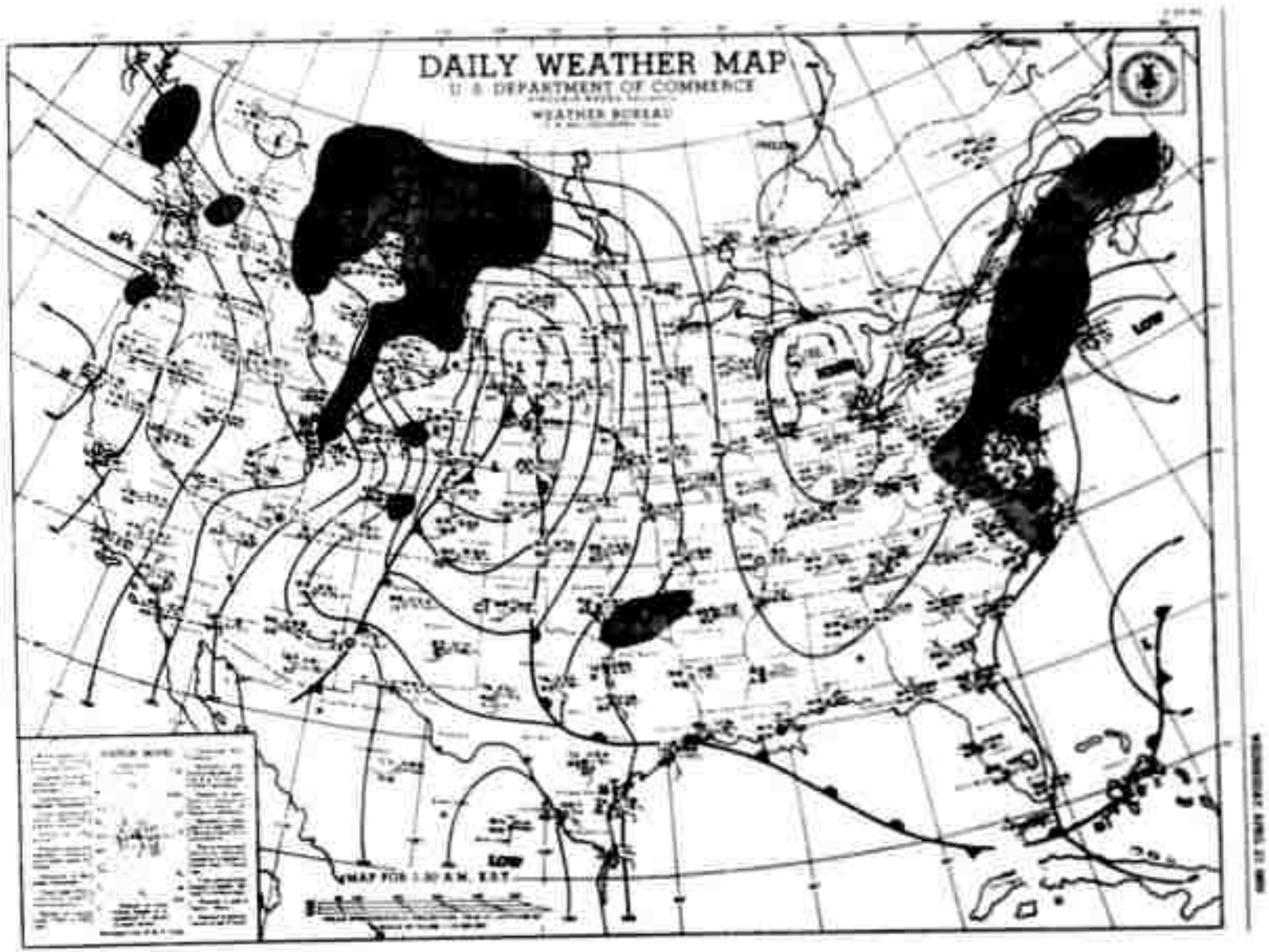

Fig. 21 SURFACE MAP, 0630Z, 27 APRIL 1955

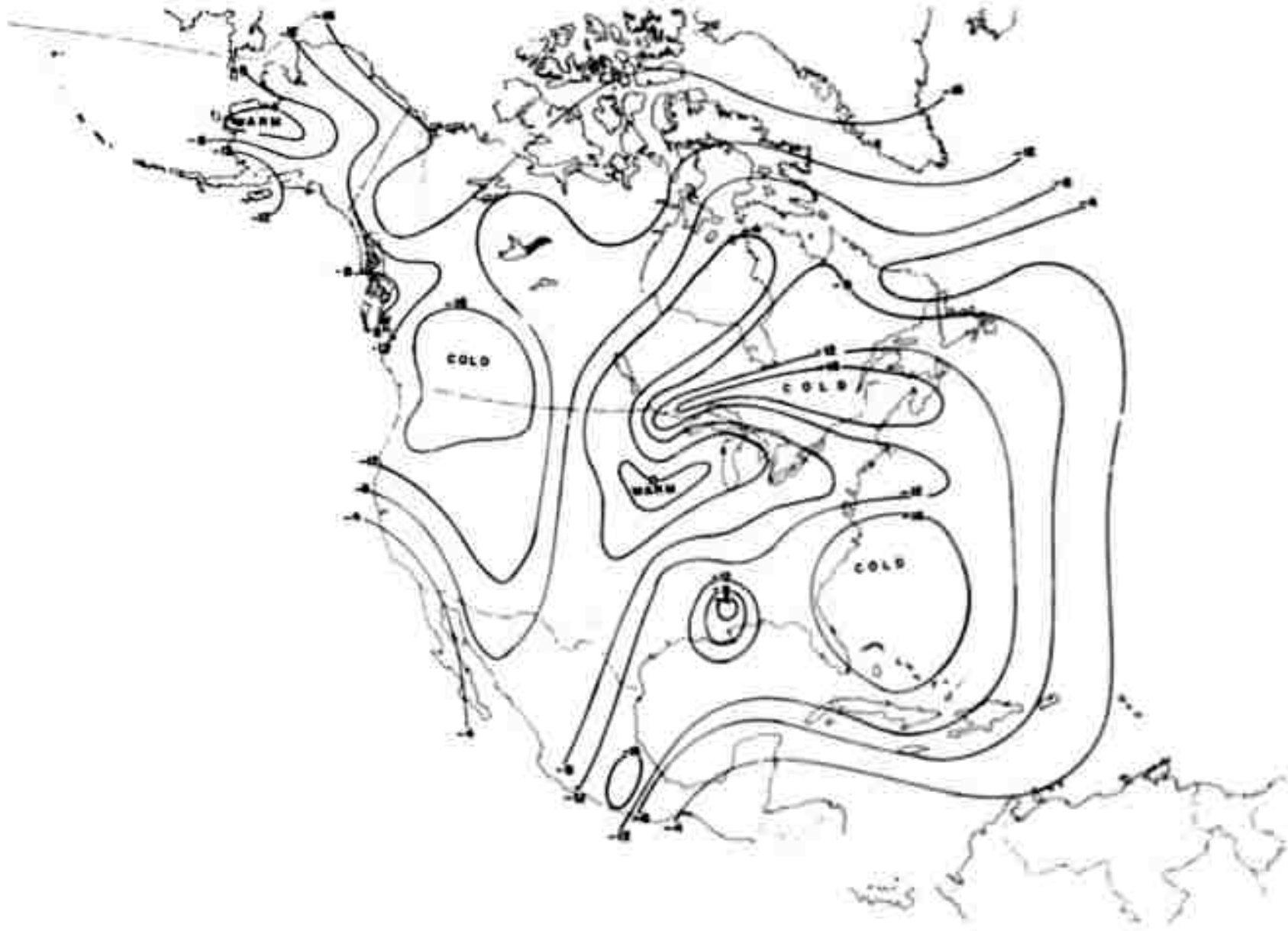

Fig. 22 0300Z, 27 APRIL 1955, TEMPERATURE AT -20° DEWPOINT SURFACE

Fig. 23 500 mb CHART, 27 APRIL 1955, 0300Z

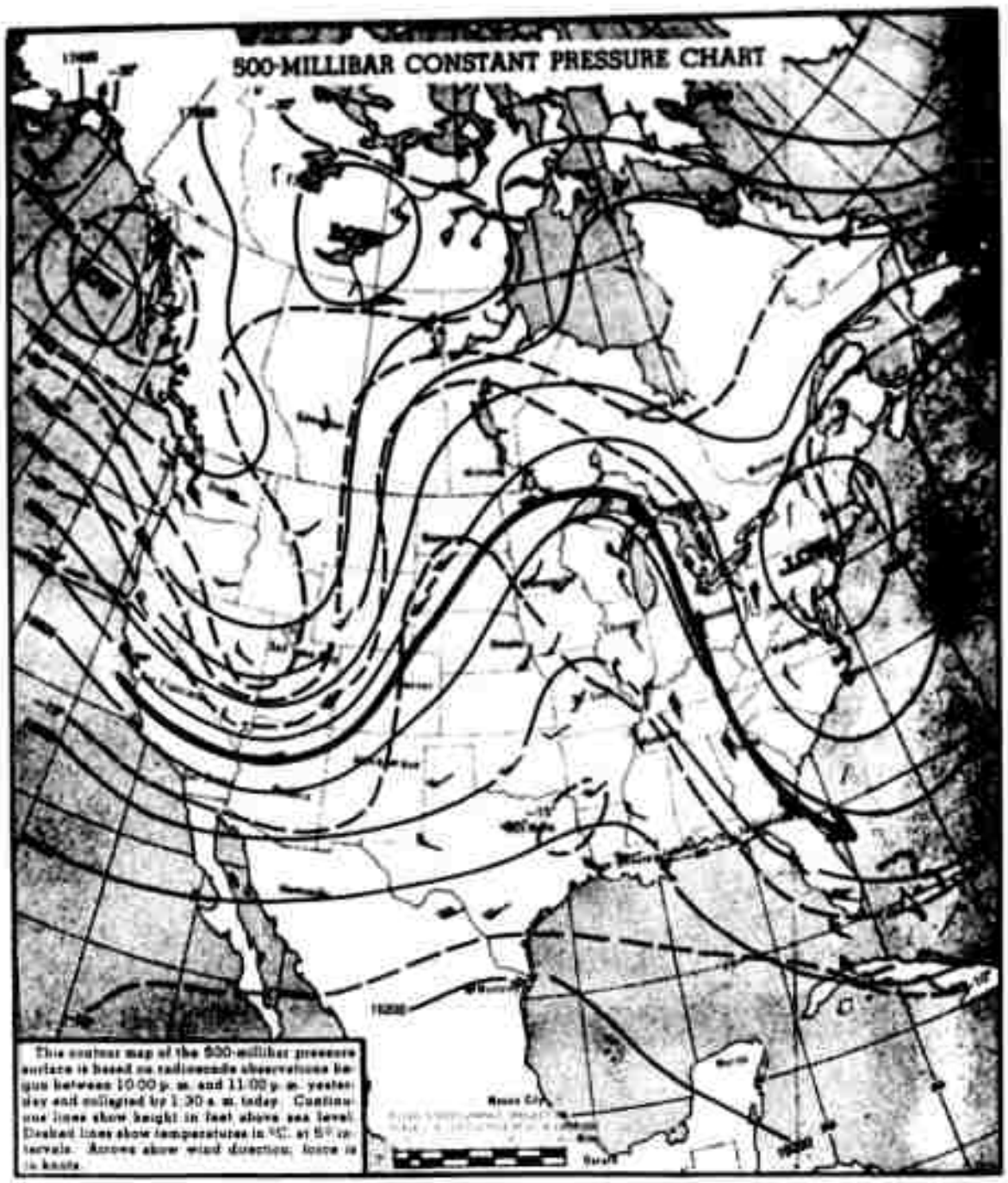

probably due to the increasingly meridional nature of the circulation which has made jet stream curvatures and meanderings too great to be followed by the loose network available for our analysis.

4.2.4.4 28 April 1955, 0300 Z

The pattern on the 0° dewpoint surface presented in Figure 24 has ceased to bear any very significant relationship to the surface chart of Figure 25. A cold area extending from Manitoba southward corresponds to the position of the low center and some of its attendant precipitation. The warm axis lies materially to the west of the surface high position. The cold area extending from New England down the Atlantic Coast apparently coincides with the areas of rain and cloudiness in those regions.

On the other hand, the 0° dewpoint surface temperature seems a strikingly good representation of the 500 mb chart given in Figure 27. The warm ridge corresponds quite nicely with the extremely sharp ridge found in the Great Lakes area. The deep trough off the coast is equally well represented. The coincidence of the Rocky Mountain trough with the ground intersection is probably fortuitous.

The -20° dewpoint surface chart of Figure 26 provides, in this case, an interesting synthesis of surface and upper air features. The same gross features that existed on the 0° chart are repeated. However, the bifurcation that was present earlier in the warm area is still marked, corresponding to the bifurcating nature of the ridge at 500 mb.

Cold areas correspond to lows and troughs. Once again, it is quite possible that even more striking similarities are obscured by details of analysis.

4.2.4.5 29 April 1955, 0300 Z

The 0° dewpoint surface chart of Figure 28 shows the path of the front across the United States marked by a cold arc. The cold center over Arkansas may represent the intersection of the front with a jet stream system crossing it at nearly right angles. A warm area over the Northern Plains States coincides with the high in the same area on the surface chart of Figure 29. The warm tongue that characterized the radiation on the Eastern side of the country has now dwindled to a thin stripe, corresponding to the collapse of the anticyclone in that area. A cold center over

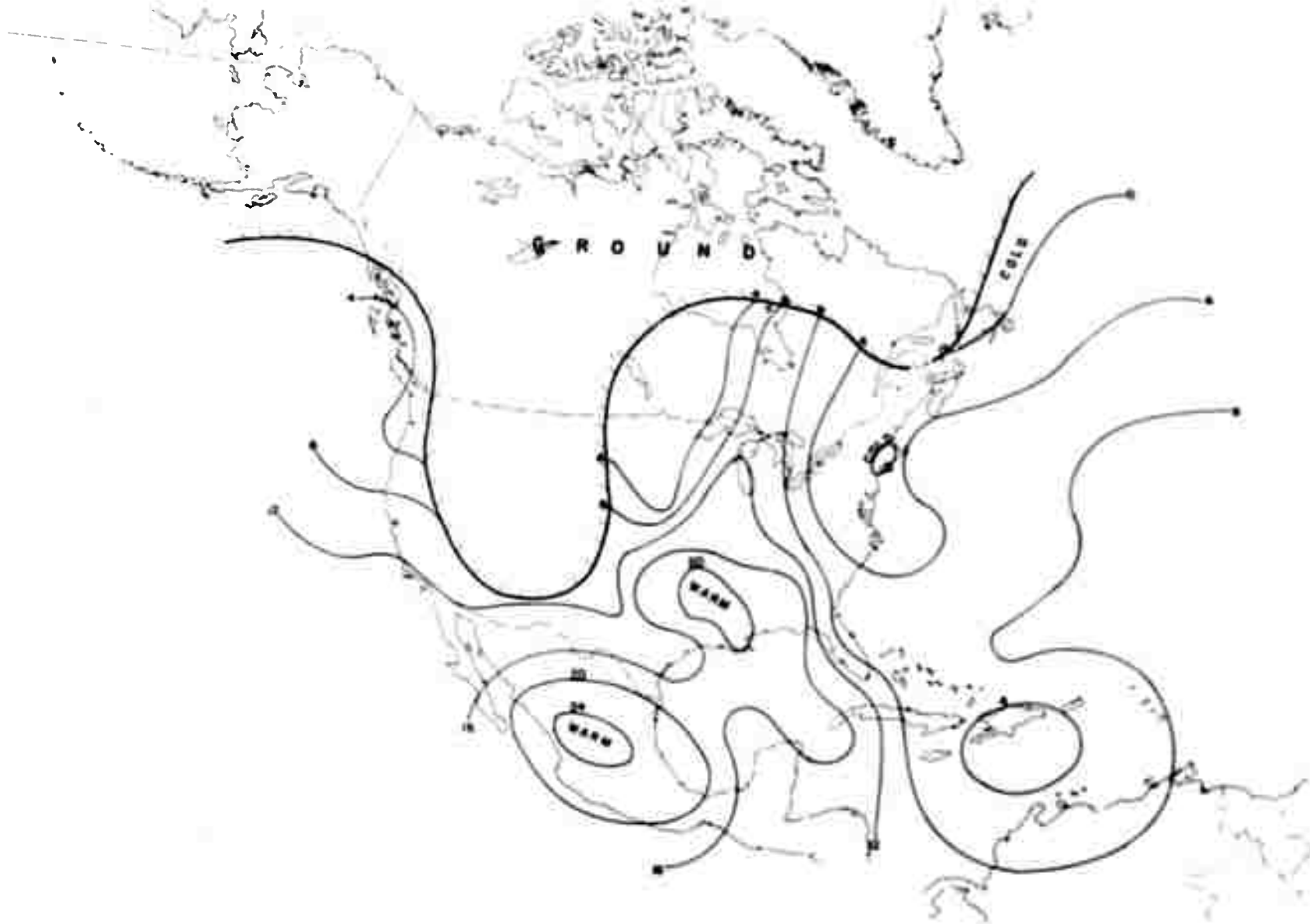

Fig. 24 0300Z, 28 APRIL 1955, TEMPERATURE AT 0° DEWPOINT SURFACE

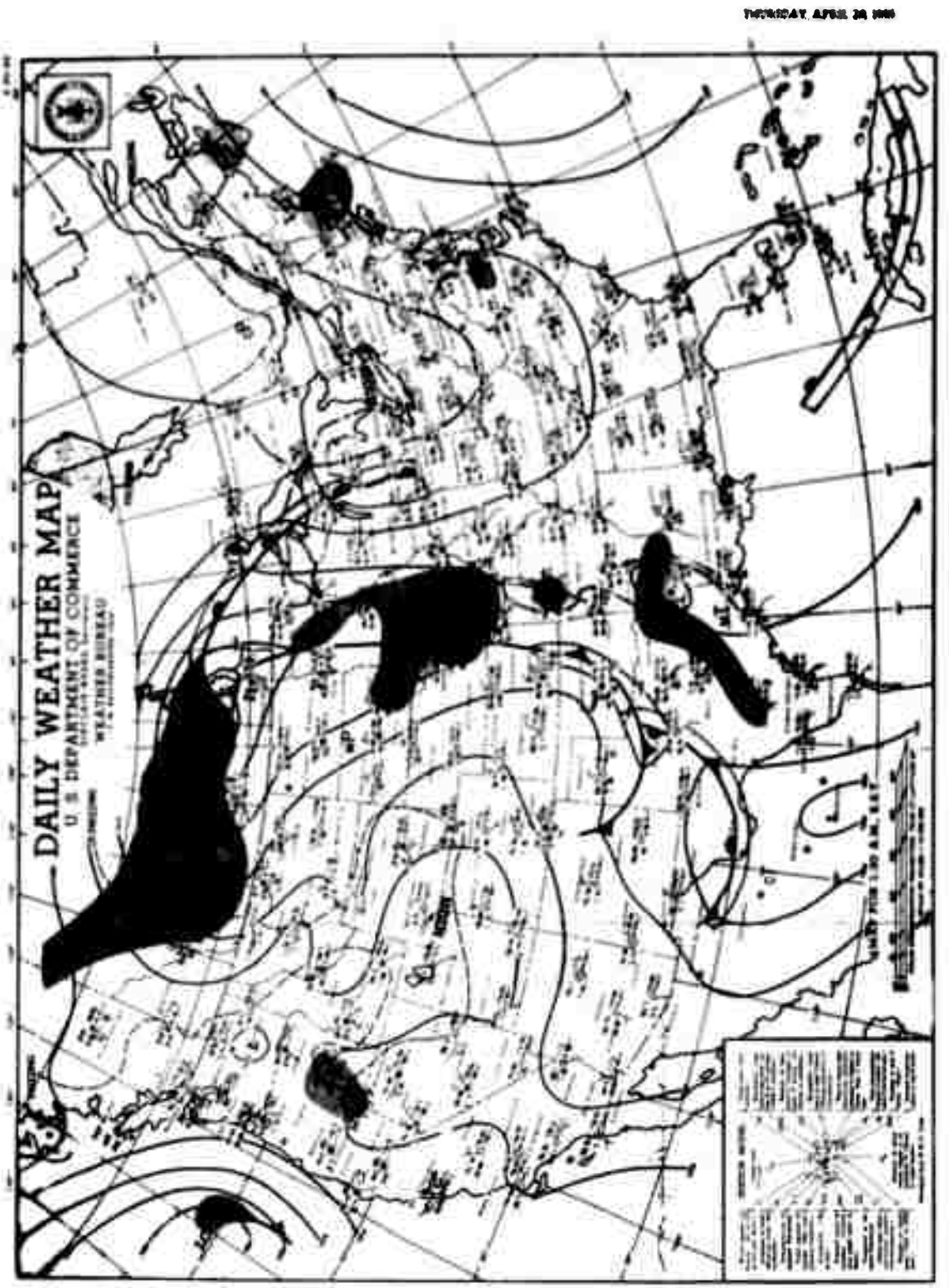

Fig. 25 SURFACE MAP, 0630Z, 28 APRIL 1955

Fig. 26 0300Z, 28 APRIL 1955, TEMPERATURE AT -20° DEWPOINT SURFACE

Fig. 27 500 mb CHART, 28 APRIL 1955, 0300Z

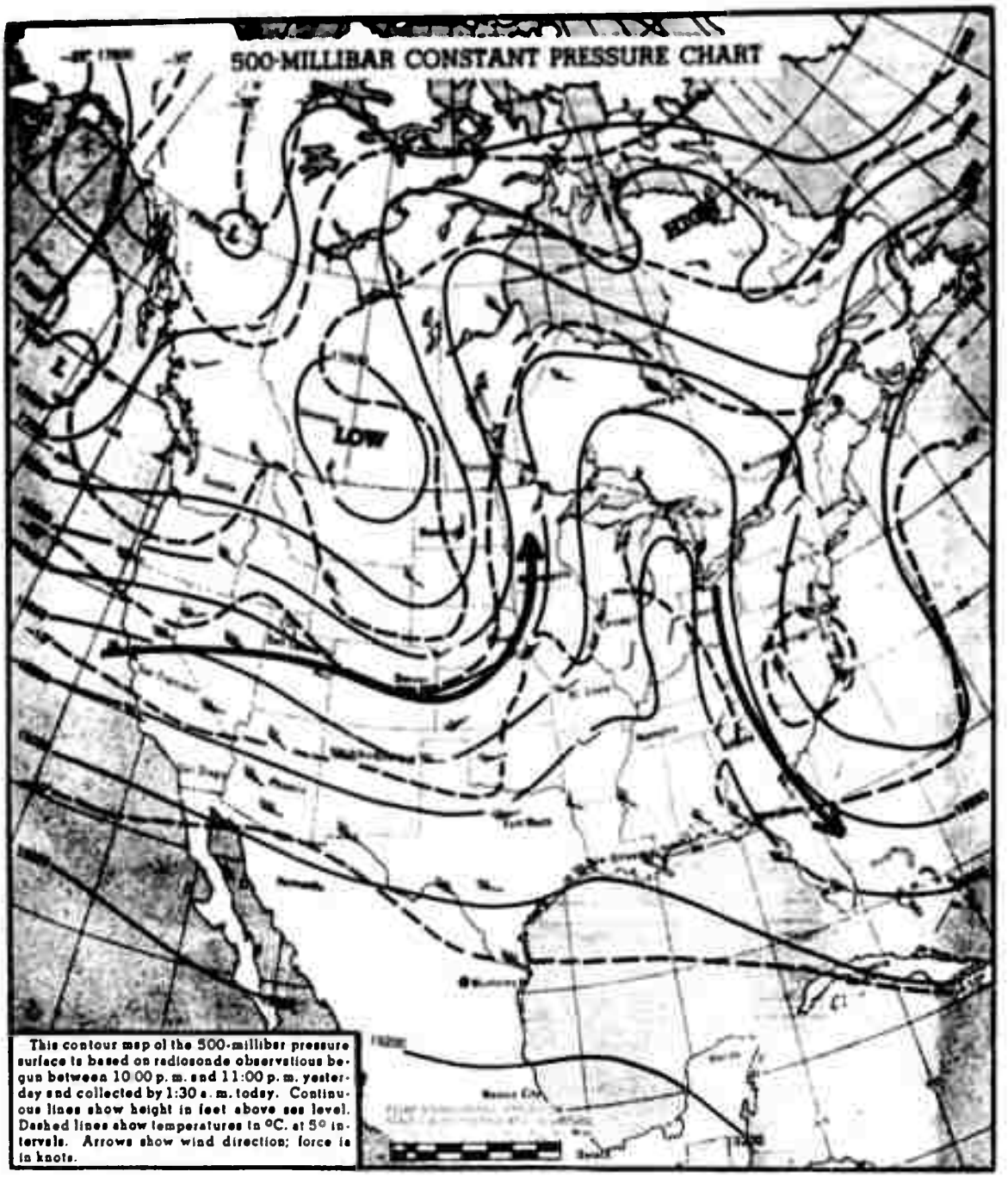

Fig. 28 0300Z, 29 APRIL 1955, TEMPERATURE AT 0° DEWPOINT SURFACE

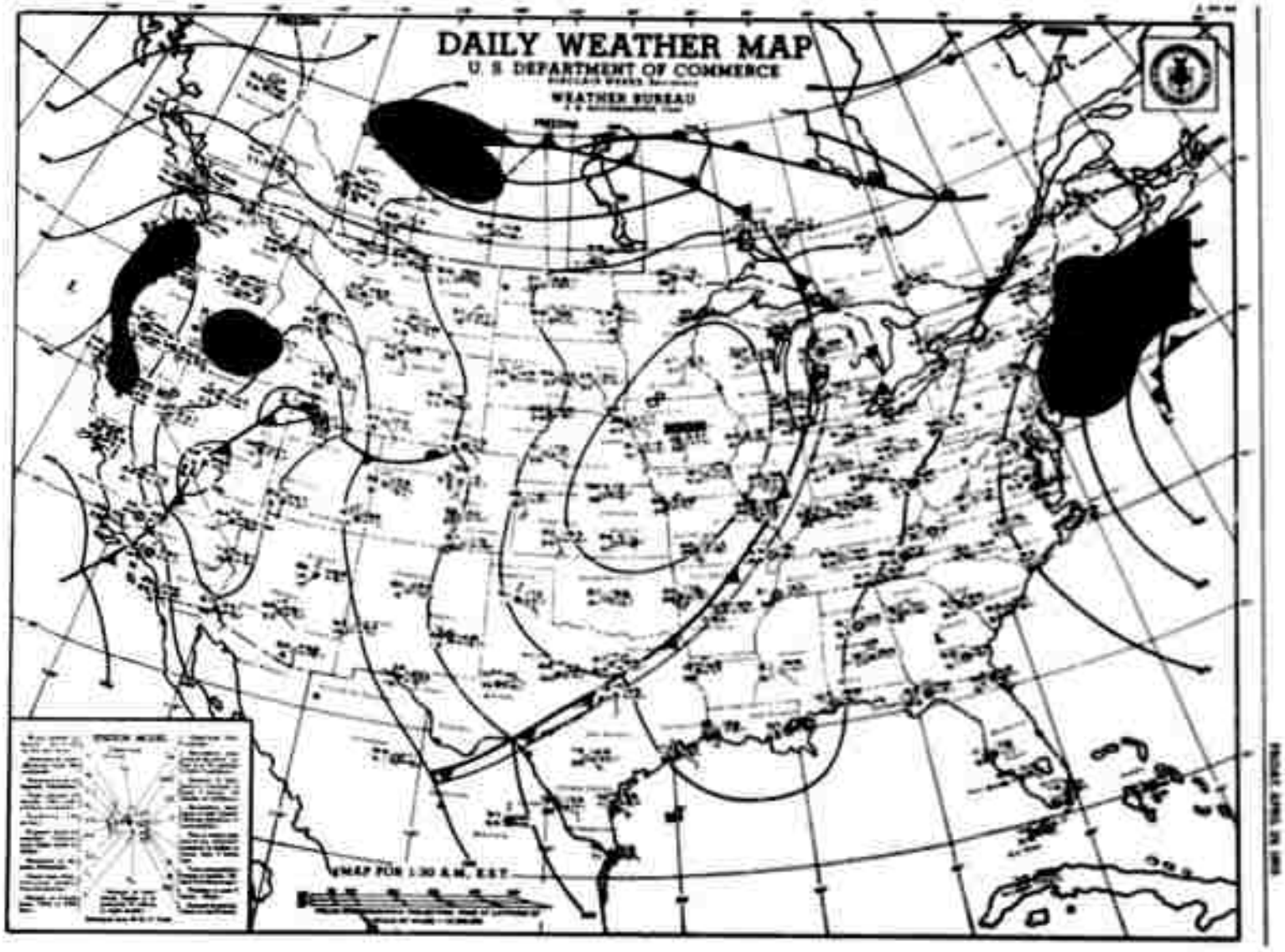

Fig. 29 SURFACE MAP, 0630Z, 29 APRIL 1955

New England corresponds to the renewed cyclonic activity in that area. A cold incursion on the Pacific Coast marks the entry of a new trough system in that area. Once again, activity in the Rocky Mountain area is obscured by ground intersection.

At the -20° dewpoint surface, presented in Figure 30, a somewhat accidented pattern is found. Insufficient data exist in the Canadian area to gain much feeling for accuracy of representation there. The split wedge has now moved to the James Bay region where it is represented by a warm center, the split still being strongly suggested. The minor southern wedges over Texas and the southeastern United States are also reasonably well represented by warm areas. The cold stripe over New England and the Maritimes is apparently related to the complicated convergent situation occurring in that area. The significance of the details over southern Florida and the Caribbean is not obvious.

4.2.4.6 Discussion

The correlation between the conventional analyses and the simulated radiation temperature maps is quite interesting. In a general sense, it appears that the high temperatures are associated with anticyclonic activity, while the low temperatures are associated with cyclonic activity. Furthermore, there does seem to be a tendency for the jet stream areas to be marked by bands of strong temperature gradient.

These findings are qualitatively similar to those obtained from a accurate calculations of the radiation from the entire 6.3μ band. This work was performed at Allied Research Associates, Inc., under Contract No. AF 19(604)-5968, and is reported in the First Semi-Annual Technical Summary Report of that Contract.

Lack of experience in the analysis of these charts has led to the delineation of structures which, in some cases, do not well correspond to features observed on the conventional charts. This lack of experience has made necessary the unquestioning use of all data points, resulting in the construction of what may be absurd gradients based on single observations. But even with these difficulties, the interrelations between conventional analyses and the temperature structure of a constant dewpoint surface seem evident.

Fig. 30 0300Z, 29 APRIL 1955, TEMPERATURE AT -20° DEWPOINT SURFACE

Fig. 31 500mb CHART, 29 APRIL 1955, 0300Z

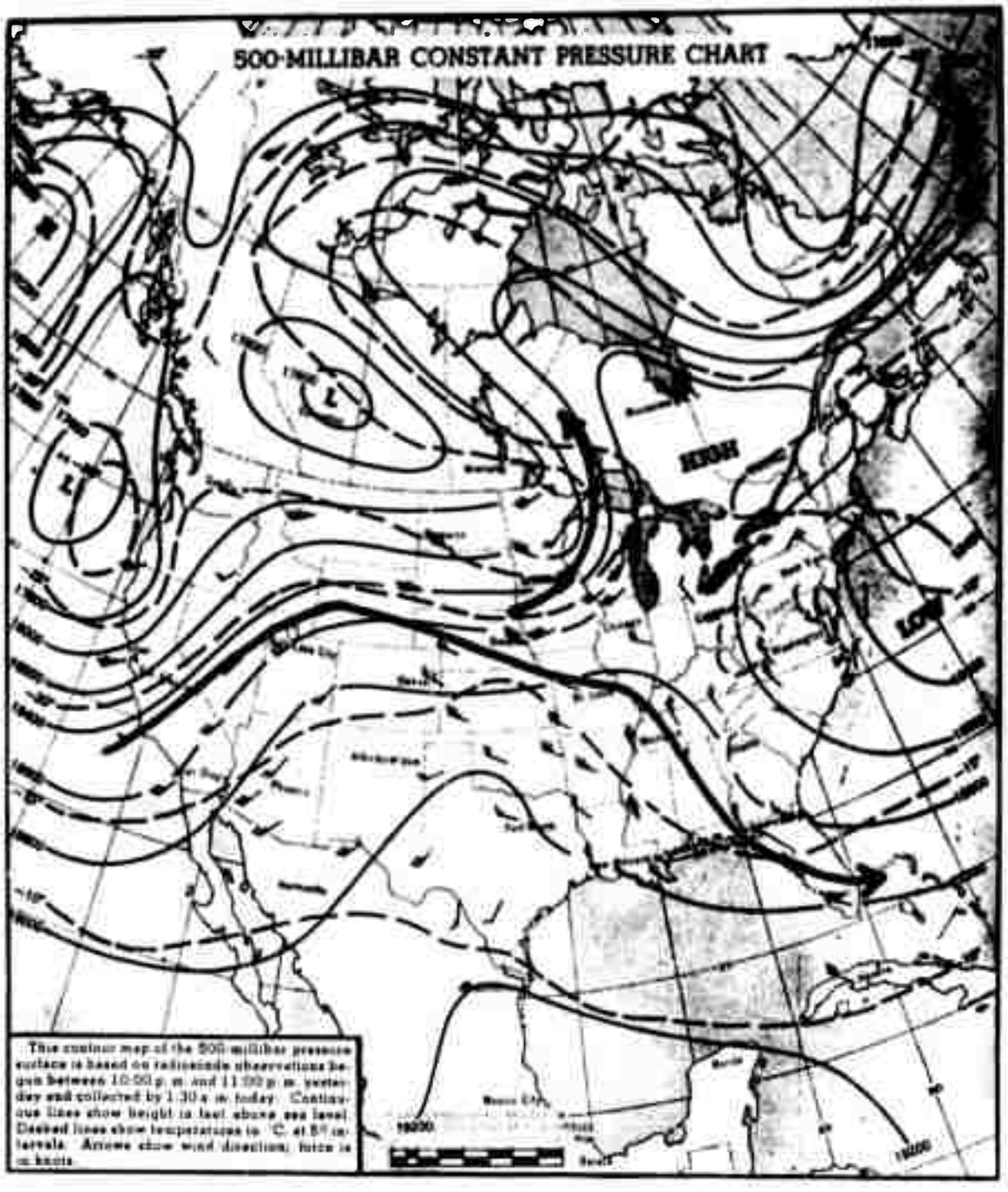

Explanation of most of the observed features is not difficult. A high temperature at a constant dewpoint surface represents a low relative humidity, which must be the result of subsiding motion in the atmosphere. Similarly, low temperatures correspond to high relative humidities where water vapor is brought up into higher (and colder) regions by upward motion. Thus, a representation of the vertical motion field is obtained, bearing the appropriate relationship to the horizontal fields of motion.

It is probably not highly profitable to pursue further the type of analysis that has been presented here. The relationships involved can be better explored by methods that take into account more of the parameters that control the amount of radiation.

The results of this analysis are interesting in that they show that observation in the infrared from a satellite vehicle can provide information that would not be available from inspection of pictures made by visible light. It also apparently demonstrates that useful results can be obtained with an infrared sensing device of extremely poor resolution.

4.2.4.7 Conclusions

To the extent that the assumptions and logic that have gone into the development of the use of constant dewpoint surfaces as surfaces of origin of radiation may be valid, it is clear that the radiating temperature of the atmosphere seen in a dense part of the water vapor emission band is a significant meteorological parameter. High temperatures appear to correspond to regions of divergence or sinking air and low temperatures to regions of convergence or rising air. This relationship is obscured somewhat by the tendency of the dewpoint surfaces to slope upward toward the south.

The results thus far obtained indicate that meteorologically useful information can be obtained from satellite observations of the infrared emission in the 6.3μ water vapor band. A considerable amount of experience and of analysis will be required before the maximum utility can be extracted from such satellite observations.

REFERENCES

1. Goody, R. M. The Physics of the Stratosphere. Cambridge University Press. 1954.

2. Godson, W. L. Meteorological Applications of Earth Satellites. Journal of The Royal Astronomical Society of Canada. Vol. 52, April 1958. p. 49-56.

3. Danjon, A. The Earth as a Planet. University of Chicago Press. 1954. p. 727.

4. Goldshlak, L., Boucher, R. J., Glaser, A. H. A Summary of the State of the Art of Cloud-Weather Relationships. Allied Research Associates, Inc. Document No. ARA-594. 4 March 1959.

5. Glaser, A. H. Meteorological Utilization of Images of the Earth's Surface Transmitted from a Satellite Vehicle. Harvard University. Contract No. AF 19(604)-1589, Phase 2. October 1957.

6. Singer, S. F. Meteorological Measurements from a Minimum Satellite Vehicle. University of Maryland, 14 January 1956.

7. Goldshlak, L., and Glaser, A. H. Development of Techniques for Meteorological Utilization of Satellite Pictures. Allied Research Associates, Inc. Document No. ARA-612. April 1959.

8. Bjerknes, J. Detailed Analysis of Synoptic Weather As Observed from Photographs Taken on Two Rocket Flights over White Sands, N. M., July 26, 1948. Rand Corporation Report No. 887.

9. Negley, R. M. On the Use of High-Altitude Cloud Photographs as a Basis for Inferring the Distribution of Wind, Temperature, Pressure and Stability. Scientific Report No. 2, Contract No. AF 19(604)-1754. Florida State University. 15 August 1958.

10. Dryden, W. A., and Prosser, N. E. Optimum Utilization of Satellite Observations in Weather Analysis and Forecasting. Final Report, Contract No. AF 19(604)-1754. Florida State University. 1 February 1959.

11. Aiken, J. J., and Widger, W. K., Jr. Measuring Cloud Velocities from a Satellite. GRD TM 57. 34. 16 September 1957.

12. Singer, S. F. and Wentworth, R. C. A Method for the Determination of the Vertical Ozone Distribution from a Satellite, Journal of Geophysical Research. Vol. 62, No. 2. June 1957. p. 299.

13. Conover, J. H. Cloud Patterns and Related Air Motions Derived by Photography, Final Report, Contract No. AF 19(604)-1589. Harvard University. June 1959.

14. Kaplan, L. D. On the Inference of Atmospheric Structure from Remote Radiation Measurements, from a paper presented at the New York meeting of the Optical Society on 3 April 1959.

15. Stakutis, V. J. and Brennan, J. X. Visibility from a Satellite at High Altitudes. "Scientific Uses of Earth Satellites". Edited by J. A. Van Allen. University of Michigan Press. 1956. p. 137.

16. Widger, W. K., Jr. and Touart, C. N. Utilization of Satellite Observations in Weather Analysis and Forecasting. Bulletin of the American Meteorological Society. Vol. 38, No. 9. November 1957. p. 521-33.

17. Wexler, H. Observing the Weather from a Satellite Vehicle. Journal of the British Interplanetary Society. Vol. 13, 1954. p. 269.

18. Dryden, W. A. Useful Satellite Orbits for Some High-Altitude Weather Observations, Scientific Report No. 1, Contract No. AF 19(604)-1754. Florida State University. 15 August 1958.

19. Elements of Map Projection. Special Publication No. 68, U. S. Department of Commerce. U. S. Coast and Geodetic Survey.

20. Hawksley, P. G. W. The Physics of Particle Size Measurement: Part II – Optical Methods and Light Scattering. Monthly Bulletin, British Coal Utilization Research Association. Vol. XVI, No. 4, April 1952.

21. Smithsonian Meteorological Tables. Sixth Edition. Smithsonian Institution. 1951.

22. Handbook of Geophysics. Chapter 16, GRD, AFCRC. 1957.

23. Murgatroyd, R. J., et. al. Some Recent Measurements of Humidity from Aircraft Up to Heights of About 50, 000 ft. over Southern England. The Quarterly Journal of the Royal Meteorological Society. Vol. 81, No. 350. October 1955. p. 533-37.

24. Kaplan, L. D. On the Pressure Dependence of Radiative Heat Transfer in the Atmosphere. Journal of Meteorology. Vol. 9, No. 1, February 1952. p. 1-12.

25. Taylor, J. H. and Yates, H. W. Atmospheric Transmission in the Infrared. Journal of the Optical Society of America. Vol. 48, 1957.

UNCLASSIFIED

UNCLASSIFIED